Size effect in heterogeneous materials analyzed through a lattice discrete element method approach

(Article begins on next page)

21 September 2024

Manuscript Details

Manuscript number	EFM_2020_353
Title	Size Effect in Heterogeneous Materials analyzed through a Lattice Discrete Element Method Approach
Article type	Research Paper

Abstract

In the Lattice Discrete Element Method (LDEM), different types of mass are considered to be lumped at nodal points and linked by means of one-dimensional elements with arbitrary constitutive relations. In previous studies on the tensile fracture behavior of rock samples, it was verified that numerical predictions of fracture of non-homogeneous materials using LDEM models are feasible and yield results that are consistent with the experimental evidence available so far. In the present paper, a discussion of the results obtained with the LDEM is presented. A set of rock specimens of different sizes, subjected to monotonically increasing simple tensions, are simulated with LDEM. The results were analyzed from the perspective of the brittleness number, proposed by Alberto Carpinteri, to measure the brittleness level of the structure under study. The satisfactory correlation between the experimental results and LDEM results confirms the robustness of this method as a numerical tool to model fracture processes in quasi-brittle materials.

Keywords	Heterogeneous Materials; Lattice Discrete Element Method; Size Effect; Brittleness Number
Taxonomy	Discrete Element Method, Mechanical Property, Numerical Computational Method
Manuscript category	All other materials
Manuscript region of origin	South America
Corresponding Author	Luis Kosteski
Corresponding Author's Institution	Federal University of Pampa
Order of Authors	Luis Kosteski, ignacio iturrioz, Giuseppe Lacidogna, Alberto Carpinteri
Suggested reviewers	Sanichiro Yoshida, Ludmila Botvina, Angelo Marcello Tarantino, Dimitrios Aggelis, Jie Xu

Submission Files Included in this PDF

File Name [File Type]

Cover Letter.docx [Cover Letter]

Response Reviewers 23-03-20.docx [Response to Reviewers]

Highlights.docx [Highlights]

EFM_update version 23-03-20.docx [Manuscript File]

declaration-of-competing-interests(3).docx [Conflict of Interest]

Marked-EFM_update version 23-03-20.docx [Supplementary Material]

To view all the submission files, including those not included in the PDF, click on the manuscript title on your EVISE Homepage, then click 'Download zip file'.

Dear Editor:

We are sending the manuscript entitled "Size Effect in Heterogeneous Materials analyzed through a Lattice Discrete Element Method Approach". This manuscript was already submitted in this journal with EFM_2019_972. We know that this new version is a new presentation of our paper, on the other hand, we could also notice that only one out of the five reviewers did not recommend our paper to be published. For this reason, we have elaborated this detailed response to our Reviewers taking into account all the observations and comments presented done before and that were really useful to help us improve this new manuscript.

In the new version of the manuscript, a deep linguistic analysis and revision in English was carried out, as well as technical observations relevant to our study. We send you an updated version of our manuscript where all the necessary changes were introduced and indicated in blue. Furthermore, our responses to the Reviewers'observations are also included, under each observation we have added our response in italic.

Best Regards,

Luis Eduardo Kosteski
Corresponding Autor
Contact Aderess: Av. Tiarajú, 810, Alegrete, RS, CEP: 97546-550, Brazil
Fone/Fax: xx55-55- 3421-8400- internal 3019
e-mail: luiskosteski@gmail.com

Reviewer Response

Ref: EFM_2019_972

Title: Size Effect in Heterogeneous Materials analyzed through a Lattice Discrete Element Method Approach

Journal: Engineering Fracture Mechanics

Comments from the reviewers:

-Reviewer 1

In the present manuscript, a discussion of the results obtained by a Lattice Discrete Element Method (LDEM) is presented. A set of rock specimens of different sizes subjected to monotonically increasing stresses are simulated. The results are viewed in the perspective of the brittleness number, proposed by one of the Authors, to measure the brittleness level of the structure under investigation.

In the following some further explanations are requested to the Authors.

(1) In the experimental results a typical shape of the body specimens are utilized, however in the numerical results a prismatic specimen (Plane Strain Condition) are considered. The comparison in terms of the brittleness number is done in these both cases. Please, discuss the influence of the specimen shape and boundary condition in the computation of the brittleness number.

In the expresion (15) presented in the paper proposed originally by Carpinteri [6,7]

$$\frac{s_E}{\left(\frac{z}{R}\right)\varepsilon_u} \leq \frac{1}{2},$$

the specimen gemometry/boundary conditions are considered by means of the slenderness relation z/R, but in the present paper this parameter is not explored. Notice that an observation about this issue was made in line 27-29 of page 16:

"The extension of the present study with the aim of verifying the influence of the slenderness, other geometric characteristics as well as other boundary conditions will be the focus of future works"

Some aspects about the LDEM Method could also be discussed:

(2) Was the influence of the mesh discretization and orientation in the results verified?

With the aim of taking into account the reviewer observation we suggest to add the following text in the second paragraph of the section 4.2. (pag. 18, line 24)

The influence of the mesh discretization is studied in Refs. [46, 60], moreover, in the simulations presented here, the discretization level is similar. In addition, in Ref. [67] was verified that the influence of the mesh rotation is marginal (less than 5%) in terms of global results and fracture configurations.

(3) Is it possible to consider more references where the validation of the numerical methodology has been carried out, showing the simulated experimental results, or the LDEM represent only qualitative results?

Several papers using this version of LDEM show in quantitative form the results. Related to this comment, in last paragraph of the introduction of the updated manuscript, we added the following text:

"…In Refs. [29-31, 36, 46, 51], LDEM simulations were discussed in which quantitative comparison with experimental results in terms of global parameters, such as displacement versus loads or final configurations, are presented."

(4) Can this method capture the size effect? Are there any other studies carried out on this topic? In which way could the random nature of the material be introduced in the model?

Yes, there are there other studies on size effect. More specifically in Rios et al. 2004 [36], among others works, size effect captured with LDEM simulations are shown. This point is mentioned in the last paragraph of the introduction:

"... the study of the scale effect in quasi-brittle materials [36-42], …"

At the beginning of page 10, we modified the text to improve the information about the introduction of the random nature of the material data in LDEM:

In the model here implemented, the random values of G_f assigned to every element have statistical independence, that is, the random properties of one element do not depend on the properties of the other neighboring elements. This assumption is equivalent to consider that the correlation length is $L_{corr} = 0.3L$. Notice that when randomness is introduced in G_f, indirectly randomness is also introduced in ε_p (see Eq. 12). In this way, the maximum strength of an element $F_{max} = EA_i\varepsilon_p$, which is directly related to point A in Figure 2, is also random. The axial stress of the element will be: $\sigma_p^* = E\varepsilon_p$.

Another alternative to introduce the random nature in the model is to consider geometric perturbation in the mesh, about this aspect see [61]. More detail about the LDEM formulation can be found in Ref. [50].

-Reviewer 2

In this manuscript, several sets of experimental and numerical results are reviewed with the aim to correlate the Carpinteri's brittleness number obtained to predict the global behavior, which is interesting for the ductile, brittle, or ductile-to-brittle transitional behavior of the fracture of non-homogeneous material. Frankly to say, the manuscript is very theoretical and must be familiar with the theory proposed by Carpinteri. The paper can be published if the following question can be answered.

1. The reference in this paper seems not so updated, the author should check whether there are new publications related to the research topic and updated them.

In the new version of the manuscript 4 new references have been added:

[67] Birck G, Iturrioz I, Riera JD, Miguel LFF. Influence of mesh orientation in discrete element method simulations of fracture processes. J Strain Anal Eng Des. 2018, 53: 6, 400-407. https://doi.org/10.1177/0309324718775284

[60] Puglia VB, Kosteski LE, Riera JD, Iturrioz I. Random field generation of the material properties in the lattice discrete element method. J Strain Anal Eng, 2019, 54: 4, 236-246 https://doi.org/10.1177/0309324719858849

[61] Iturrioz I, Riera JD, Miguel LFF. Introduction of imperfections in the cubic mesh of the truss-like discrete element method. Fatigue Fract Eng M. 2014, 37: 5, 539-552. https://doi.org/10.1111/ffe.12135

[70] Birck G, Rinaldi A, Iturrioz I. The fracture process in quasi-brittle materials simulated using a lattice dynamical model. Fatigue Fract Eng Mater Struct. 2019, 42: 12, 2709-2724. https://doi.org/10.1111/ffe.13094

2. The highlights of this paper should be emphasized to make clear the contribution of this paper.

The highlights were rewritten in order to take into account the Reviewer's observation

Carpinteri´s brittleness allows to identify specimen ductile-brittle global behavior.

Several experimental and numerical uniaxial tensile tests are done to verify the brittle number classification.

The use of this version of Lattice Element Method allows capturing the damage process in quasi-brittle materials.

This version of Lattice Element Method uses the brittleness number to calibrate the input parameters.

3. The format of references is not uniformed and should be rechecked.

All the references have unified as indicated in the Guide for Engineering Fracture Mechanics Journal.

-**Reviewer 3**

This paper uses Lattice DEM to investigate size effects in brittle/ductile behavior. The paper is centered around the brittleness number, (a variation of flaw tolerance numbers defined in the classical Dugdale–Barenblatt model).

The subject is clearly of interest to Engineering Fracture Mechanics but the manuscript has too much weaknesses to be considered for publication. I list hereafter a series of problems that I found in the paper, which overall support my recommendation to reject the paper.

The main weakness of the paper is that it is badly written. Consequently, it is very difficult to understand. The authors have not been careful in checking their manuscript for readability and English correctness. They should have given their manuscript to someone well versed in English. It should be a natural courtesy to the reviewer (and to the potential reader) to fix these issues before sending (too quickly) their manuscript. Overall the analysis is not of sufficient quality and does help in understanding the experimental results (in particular in relation with the brittleness number).

In the new version, we have improved our writing in English and we expect that the text could be understanding for the Reviewer.

Next, we will try to reply to the technical questions and propose some modifications in the text in order to improve the quality of our work by following the Reviewer's observations:

Many statements are very unclear such as:

'*Despite this recommendation, in the present work the number S; is used in the context of quasi-brittle materials because it allows to emphasize some particular aspects related to the simulation results obtained with the lattice discrete element method.*'

In the new version of this manuscript, this statement was replaced by the following one:

In the present work, the s instead of s_E parameter was used to measure the change of global behavior in the specimens that were tested and consequently simulated by the model.

Fig. 2 seems to indicate that the local model cannot induce failure in tension. However the authors state that:"In this way, the failure in compression is induced by indirect traction".

Considering Figure 2, which represent the local constitutive law F vs. strain, if the path is, e.g., OAP, the element is damaged. The local relationship for bars subject to compression has a linear behaviour.

Introducing the fracture energy as a random field, the random nature of the material can be considered. This behaviour produces also random characteristic strain ε_p at a local level, and causes that, when a generic bar (i) is subjected to compression, the tensile strain generated by the Poisson effect in the weaker transversal bar situated close to the i-bar, reach the ε_p value beginning to damage.

This process triggers the damage process and allows the structure to collapse. In quasi-brittle materials such as ceramic, rock, concrete, etc, where the tensile strength is about 1/10 times the compression strength, the mechanism described above is compatible with the experimental evidence.

In several papers carried out with a similar LDEM model, interesting quantitative results in terms of global strength vs. displacement curves and final configurations have been obtained. See, among others [30,46].

More generally, I found that it was very difficult to understand the model because the separation between local (elements) and macroscopic parameters is not clearly stated. The authors should have more clearly postulated which parameters are local and which are global.

This model of LDEM was explained in several papers published in several well-known journals. See for example:

[30] Kosteski LE, Iturrioz I, Cisilino AP, Barrios D'ambra R, Pettarin V, Fasce L, Frontini P. A lattice discrete element method to model the falling-weight impact test of PMMA specimens. Int J Impact Eng. 2016, 87, 120-131. https://doi.org/10.1016/j.ijimpeng.2015.06.011

[50] Birck G, Iturrioz I, Lacidogna G, Carpinteri A. Damage process in heterogeneous materials analyzed by a lattice model simulation. Eng Fail Anal. 2016, 70, 157-176. https://doi.org/10.1016/j.engfailanal.2016.08.004

[51] Da Silva GS, Kosteski LE, Iturrioz I. Analysis of the failure process by using the Lattice Discrete Element Method in the Abaqus environment. Theoretical and Applied Fracture Mechanics. 2020, 107, 102563. https://doi.org/10.1016/j.tafmec.2020.102563

[60] Puglia VB, Kosteski LE, Riera JD, Iturrioz I. Random field generation of the material properties in the lattice discrete element method. J Strain Anal Eng, 2019, 54: 4, 236-246 https://doi.org/10.1177/0309324719858849

In some previous reviews of our works, we were criticized because we have the tendency to repeat the explanation of the LDEM formulation. However, and in order to improve our paper, we have considered the reviewer's observation, thus, we have introduced lines 11-12 in page 10:

"...More detail about the LDEM formulation can be found in Ref. [50]."

We have also modified the text on page 11 lines 10-20:

The LDEM model considers the following macroscopic parameters: the elastic modulus E, the fracture energy G_f, and the characteristic length d_{eq}. With these three parameters using Eq. (12), the critical strain ε_p, where the bar force reaches its maximum value is computed (see Fig 2). Multiplying E by the Eq. (3) and (4) the linear pre-peak relation in the elemental constitutive law (ECL), defined by EA_i, is indicated in Figure 2. The fracture energy G_f directly influences in the area below the ECL, as it is indicated in Eq. (6). Furthermore, using Eq. (13) as illustrated in Fig. 2, the characteristic length of the material, d_{eq}, defines the post-peak branch in the ECL by means of the local parameter ε_r. Notice that not only ε_r, but also EA_i depend on the discretization level.

The authors state that '*a very clear brittle behavior could be defined when;is lower than 1, as seen for the F(= 0.74) specimen in the FELSER set.*' And reiterate this kind of statement on all the experimental curves. However, I made a quick (and anonymous) blind test (only showing the Force/displacement curves) to several colleagues in my department asking

them to point out which curve is ductile and which is 'clearly' brittle in Tables 1, 2 and 3. None of them (like me) was able to discriminate brittle and ductile behaviors. This is problematic as it shows that the criterion used for experiments on which the authors base their analysis (and model) is not sound enough.

To clarify the Reviewer's observation we propose to introduce the following paragraph on pages 15 and 16, right below Table 4:

With the aim of categorizing the global behaviors in all the tests carried out, a typical brittle global response it is considered when:
a) considering tests under controlled displacement, after reaching the peak load, the global displacement is smaller than that corresponding to the peak load. As in the case of the (F) specimens of the FELSER sandstone set presented in Table 2;
b) considering tests under force control, after reaching the peak load, the behavior is characterized by a clear jump in the load, without any significant softening branch. The specimen (D), presented in Table 4, is an example of this second case.
On the other hand, a typical ductile global behavior is considered when the global post-peak displacement is higher displacement corresponding to the peak load. The Felser tests from (A) to (C), presented in Table 2, are clear examples of this kind of global behavior.

Fig. 7, which is based on LDEM simulations is much clearer in this regard. It makes sense that the model leads to a better discrimination between brittle and ductile behaviors as it is based on simplifying assumptions. However, here the reader is left with the feeling that the experimental part does not support clearly the simulation results. In this respect, the fact that the critical value of s takes different values depending on the analysis (s= 0.7, 1, 1.5) does not clarify matters.

As a response to the Reviewr's obersvation, we have added in the updated manuscript a new figure and the following comment on pages 21-22:

The experimental and numerical results in terms of the brittleness number s, and global behavior (brittle-ductile transition), are shown in Figure 8. A global brittle behavior is considered if s is smaller than 0.7, a ductile one if s is higher than 1.5. A transition can be considered if s is comprised in the interval [0.7, 1.5]. It should be noted that $s < 0.7$ is a lower bound, but tests with brittle global behavior can occur with values above this limit. Furthermore, the ductile transition limit $s > 1.5$ shows a certain level of dispersion. The specimen shape and the influence of boundary conditions could be responsible for this dispersion. But despite this behavior, the limits $s<0.7$ and $s>1.5$ identify that the typical brittle-ductile transition take place in the specimens.
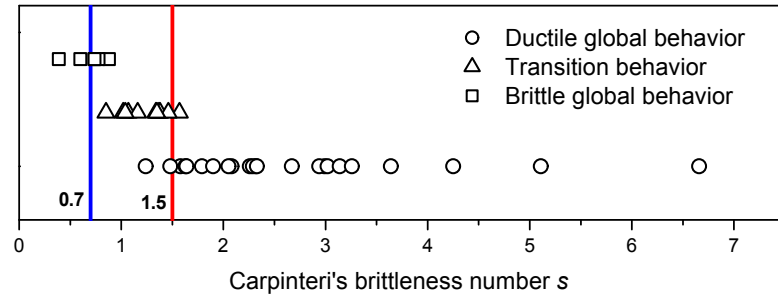
Figure 8: Representation of the *s* values in experimental and numerical results.

I found that the coefficient of variation of Gf very arbitrary. No explanation for its value (or range of values) is given. The randomness of the simulated structure comes from this parameter and is thus of importance.

In other works presented by the authors values of CV(Gf)=40-50 % were used, with the aim to represent the behaviour of quasi-brittle material. In the Kosteski's Ph.D. Thesis [68] an exhaustive parametric study of the variability of Gf was carried out. Moreover, in several works developed by two of the authors of this paper, the influence of the fracture energy variability and other related aspects, such as the random nature of the material, are presented by using LDEM [30, 60, 61]. In the present paper simulations with different, CV(Gf) have been performed to study the sensitivity of s to Gf parameter.

Taking into account the Reviewer's observation, we introduced the following sentences, on page 24 after Fig. 10, in the updated manuscript:

In Figure 11, it is possible to verify in which way the variability of the fracture energy CV (G_f) influences the brittleness number *s* computed using the LDEM formulation. The simulations presented in section 4.1 were carried out using CV (G_f)=40%, this value is usually employed to simulate quasi-brittle materials such as concrete and rocks (see e.g. [36], [38]). Moreover, a particular study about the influence of the variability CV (G_f) was conducted in [30].

The sentence '*In this study, simulations with similar rupture pattern were used, specifically, those simulations of specimen in which at the end only one fissure propagated.*' Is problematic why would simulations with several cracks be discarded?

Down below, a figure that illustrates the difference between a plate where the localization process happens in one (blue line) or two cracks (red line) is represented. By this figure it is possible to understand the hight influence of this aspect in the shape of the post-peak curve. In our paper, the brittle-ductile transition behavior, by comparing the shape of the force vs. displacement responses, is defined; for this reason, it was avoided to consider the influence of other factors. This aspect could be analyzed in other research papers. In the present paper, are taken into account simulations were only one crack propagates in the collapse configurations. In the experimental results, no information was documented about this aspect. In Kosteski [68] this aspect was preliminarily studied.
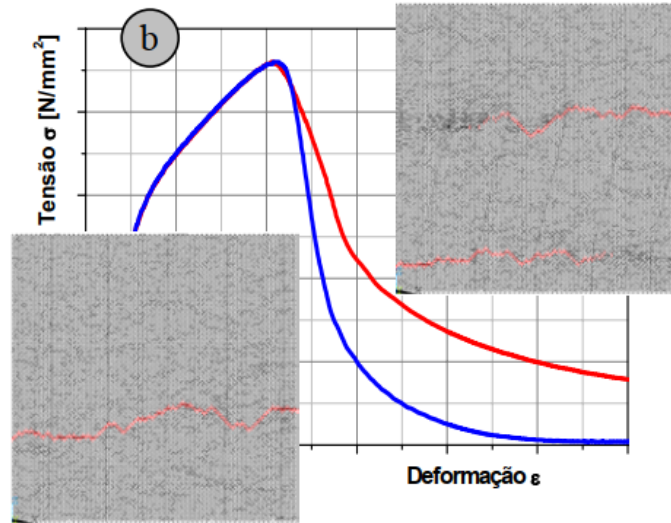
Figure: Source [68]. Global curves LDEM simulated

With the aim of taking into account the Reviewer's consideration, we have added some new sentences in the first part of page 21.

The simulations resulted in different fracture patterns that in some cases produced one, two or more cracks. It is worth noticing that the auto-similar configuration was used throughout this work. For this reason, simulations, in which only one macro-crack propagate, were considered. As it can be seen in Figure 5, b = 3.5m, there is more than one crack in the final configuration, but the other cracks or its bifurcation become stable and do not propagate to broke the specimen. When more than one crack propagates, the stress-strain curves present a different morphology.

I list a non-exhaustive list of sentences that at least unclear, grammatically incorrect or using incorrect words (fissure does not seem like the proper word for cracks in a journal like Engineering Fracture Mechanics).

For each case other alternative sentences, reported below, have been included in the new manuscript version.

1-The element constitutive relationship, presented in Figure 2, is defined in terms of parameters depending on the material, parameters () that do not depend on model discretization, and parameters () depending on the material properties and/or the model discretization.

The indicated sentence has been replaced the by the following one:

The LDEM model considers the following macroscopic parameters: the elastic modulus E, the fracture energy G_f, and the characteristic length d_{eq}. With these three parameters using Eq. (12), the critical strain ε_p, where the bar force reaches its maximum value, is computed (see Fig 2). Multiplying E by the Eq. (3) and (4) the linear pre-peak relation, in the elemental constitutive law (ECL), is defined by EA_i, as indicated in Figure 2. The fracture energy G_f directly influences in the area below the ECL, as is indicated in Eq. (6). Furthermore, using Eq. (13) as illustrated in Fig. 2, the characteristic length of the material, d_{eq}, defines the post-peak branch

in the ECL by means of the local parameter ε_r. Notice that not only ε_r, but also EA_i depend on the discretization level.

2-The deduction of this expression could be founded in

We have replaced this sentence for:

This deduction can be found in [45].

3-the critical fissure of size

We have replaced this term for:

The critical crack size

4-specific facture energy

We have replaced this term for:

fracture energy

5-in the head of the fissure

We have replaced this term for:

In the crack tip

6-a region of the dominium

This expression has been replaced by the following one:

a dominium portion

7- are statistical independent

This expression has been replaced by the following one:

Have statistical independence

8-Another interesting feature of the method is that, although it uses a scalar damage law to describe the uniaxial behavior of the elements, the global model accounts for anisotropic damage, since it possesses elements orientated in different spatial directions.

The previous sentence has been replaced by this other:

Another interesting feature of the method is that, although it uses a scalar damage law to describe the uniaxial behavior of the elements, involves a global model that takes into account of the anisotropic damage. This is because, when the uniaxial bars, oriented in different directions, are damaged they modify their axial stiffness, allowing to represent an anisotropic global behavior.

-**Reviewer 4**

The paper is devoted to the important problem of the influence of the size of a sample from concrete and rocks on the mechanical properties of these materials. To analyze the size effect, the authors used the Carpinteri's brittleness number estimated using literature experimental data for concrete, polystyrene, and rocks, as well as a numerical analysis method, the results of which showed a good agreement with the experimental data. The study is important both from a scientific and an applied point of view and can be recommended for publication taking into account the following comments.

1. As a parameter of brittleness, the authors used a coefficient in a known ratio connecting the specimen size with a parameter characterizing the size of the process zone. The authors know for sure that for the first time, requirements for the specimen size were proposed in [R.W. Boyle et al. Welding J. Research Suppl., 41, 428s (1962)], which were based on introduction of the correction for the plastic zone under plane deformation, and the ratio of the specimen thickness to the size of the zone was taken equal to 4.

Further this ratio was taken equal to 2.5 [W.F. Brown Jr. and J.E. Srawley, ASTM Special Technical publication, No.410, (1966)], and it was noted that testing samples without cracks to establish requirements for sample sizes lead to erroneous results.

In following works carried out on metals, this coefficient was refined by experimentally estimating the size of the plastic zone and studying the microrelief of fracture surfaces allowing it to be associated with the fracture mechanism. The value of specimen thickness was always taken as the specimen size, since its change has the largest effect on the change in the stress state.

In other words, there is a large history of the question of the coefficient in a known ratio relating the specimen size to a parameter characterizing the size of the process zone. It would be desirable if the authors briefly reflected this story in their paper.

We agree on the above comments of the Reviewer, and in order to take into account his observations, we propose to introduce new sentences in the updated manuscript, more specifically, in the first introductory paragraph:

In the literature, the scale effects were extensively studied to connect the fracture process zone with the specimen size, the pioneer works of Dugdale [1], Boyle [2], and Brown and Srawley [3] could be cited among others. More specifically, in the so-called quasi-brittle materials, such as concrete, this topic was also widely discussed. This kind of materials are chararacterized by a disordered microstructure, exhibits damage localization, and are unable to present plastic or hardening deformations, having a non-negligible fracture process zone

compared to the structure size. Furthermore, it was observed that the structural behavior changes with the size of the analyzed specimen.

[1] Dugdale DS. Yielding of steel sheets containing slits. J Mech Phys Solids. 1960, 8:2, 100-104. https://doi.org/10.1016/0022-5096(60)90013-2.

[2] Boyle RW, Sullivan AM, Krafft JM. Determination of plane strain fracture toughness with sharply notched sheets. Welding J Res Suppl. 1962, 41, 428-432.

[3] Brown Jr WF, Srawley JE. Plane strain crack toughness testing of high strength metallic materials. ASTM Special Technical publication, No. 410, ASTM, Philadelphia, Pa. 1966.

2. It is not always clear from the text of the paper which criterion the authors use when dividing tensile diagrams into those corresponding to brittle, quasibrittle and ductile failure.

To clarify this Reviewer's observation, we have added the following paragraph, on page 15 below Table 4:

With the aim of categorizing the global behaviors in all the tests carried out, a typical brittle global response it is considered when:
a) considering tests under controlled displacement, after reaching the peak load, the global displacement is smaller than that corresponding to the peak load. As in the case of the (F) specimens of the FELSER sandstone set presented in Table 2;
b) considering tests under force control, after reaching the peak load, the behavior is characterized by a clear jump in the load, without any significant softening branch. The specimen (D), presented in Table 4, is an example of this second case.
On the other hand, a typical ductile global behavior is considered when the global post-peak displacement is higher displacement corresponding to the peak load. The Felser tests from (A) to (C), presented in Table 2, are clear examples of this kind of global behavior.
When it is not possible to define a clear brittle, or ductile behavior, we consider this case as a global transition behavior, see, for example, specimen (A) of the Polystyrene specimens presented in Table 4.

So, it is not clear why the diagrams given in Tables 1 and 2 are classified as ductile or quasibrittle. Diagrams of the specimens with different sizes remain similar to each other.

In Table 1, only ductile and global transition behavior appear. In Table 2 a brittle behavior of the F specimens for the FELSER sandstone case is represented; moreover, transition and ductile global behavior appear in this set of tests. We believe that, with the description presented immediately above, the identification of brittle-ductile transition behavior will be easy to understand. In addition, in the new version of the manuscript, Figure 8 has been added to illustrate and better clarify the proposed classification. In this figure, all the tests presented in the paper have beeen categorized in function of the parameter s and the global aspect of the curve force vs. displacement response.

A decrease in the number of brittleness is obvious, however, the displacement and the fracture work corresponding to the area under the diagrams are not reduced, there is no information about the microrelief of fracture surfaces.

Establishing a comparison between the area below the force vs. displacement is not possible, and at least not directly. To carry out this comparison, we need to normalize this area with respect to its characteristic structural dimension. Notice also that, when the global behavior is brittle (if the displacement is not controlled during the test), the area under the force vs. displacement curve is not proportional to the released energy. In the instability branch, we have an interaction between dissipated-elastic and kinetic energy. See the following figure that illustrates this explanation. About the information of microrelief of fracture surface and final configuration aspect, some information about this topic was carried out in other works referenced below.
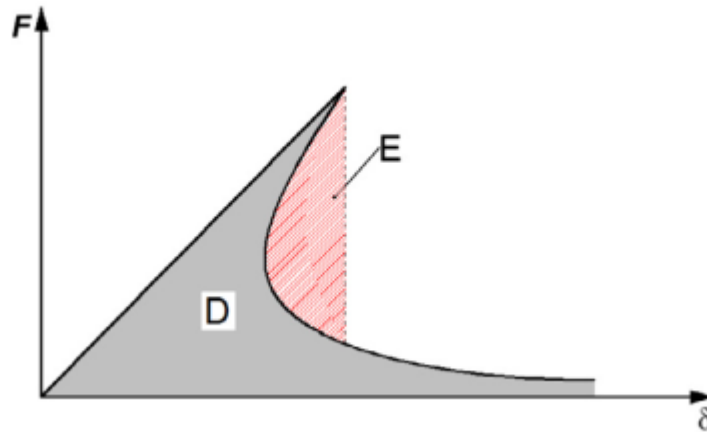
Figure: The generic global Force vs displacement response is presented, where D indicates the energy below the curve which is proportional to the dissipated energy, and E indicates the kinetic energy. If the displacement δ is not controlled, the area below the curve, representing the total released energy, is proportional to D+E. Source: A. Carpinteri, G. Lacidogna, M. Corrado, E. Di Battista. Cracking and crackling in concrete-like materials: A dynamics energy balance. Engineering Fracture Mechanics 155 (2016) 130–144. http://dx.doi.org/10.1016/j.engfracmech.2016.01.013

As regards the Reviewer's comment, we propose to add, in the updated version of the manuscript, the following paragraph on page 26, immediately before the conclusion:

In the present paper, a comparison between the global specimen behavior during damage process and the brittleness number is established. In [42],[50],[70] the link of the brittleness number with the dissipated energy and the final configurations obtained with LDEM simulations was also studied.

3. It would be desirable to present at the beginning of the paper the nomenclature of accepted designations.

In the updated version of the manuscript a nomenclature used in the paper was included.

-Reviewer 5
- Interesting paper. Maybe a revision for language issues would be suitable.

A detailed revision and correction of the language used in this manuscript was made.

1. Check in the 1st highlight the last name: "Carpintieri"?

This was corrected.

2. Also, instead of "let" I would suggest "allows to"

This was corrected.

3. 2nd highlight: "A version of a lattice element method use the brittleness number to explain their input parameters." Should be "uses" (not "use") but anyway this highlight is not very descriptive for the reader, could be replaced.

The highligths were replaced

4. Can (and how) the porosity be taken into account? Different diameters etc.

In the LDEM, it is possible to build the topology of the porosity by eliminating elements in certain specific regions mimicking the topology of the pores. On the other hand, the porosity could be simulated as a random damage field. As regards how to induce different types of random fields in LDEM see in:

[60] Puglia VB, Kosteski LE, Riera JD, Iturrioz I. Random field generation of the material properties in the lattice discrete element method. J Strain Anal Eng, 2019, 54: 4, 236-246 https://doi.org/10.1177/0309324719858849

5. It is interesting that in Table 7, the increase of size results in increase of the variation coefficient but to stable strength values. Could the authors discuss this in more detail?

Taking into account the Reviewer's observation, we propose to add the following sentences in the paper, more specifically, on page 22, lines 16-23.

In Fig. 9(a), it is clear that the size effect in the global ultimate stress is practically null. This effect could be seen in the values presented in Table 7. The difference between the maximum and minimum values of mean global stress is 1.23% and the variation coefficients do not exceed 1.64%. The sensitivity of the global parameters with the size effect depends on several factors, such as the boundary conditions, and the random nature of the material input data. In Rios and Riera [36] experimental tests with different geometries and boundary conditions were simulated with LDEM, and the values of strength and its variability are reached with success.

6. In addition, why do the authors present the "displacement" and not the "strain"? Displacement will anyway be different since the specimen length changes.

All the experimental results presented in this paper and taken from the literature were showed in terms of displacement. For this reason, LDEM results were presented in this format.

7. Concerning the spontaneous fracture: does this model indicate that correlations may emerge between acoustic emission parameters and the final

strength like it was shown experimentally in [Mpalaskas et al. Mechanical and fracture behavior of cement-based materials characterized by combined elastic wave approaches, Construction and Building Materials, 50, 2014, Pages 649-656]?

Several works were presented by the authors about this topic. The LDEM method has shown skillfully how it is capable of simulating acoustic emission tests. Some of the authors published works as Ref. [34, 35, 48-50] using LDEM to simulate AE events. In the manuscript, the possibility of LDEM to simulate the acoustic emission tests is presented at the end paragraph of page 4.
The reference indicated by the reviewer is very interesting, thanks for the suggestion.

"…and finally the acoustic emission events in quasi-brittle materials [34, 35, 48-50]."

To taking into account the reviewer observation we modified the last paragraph of the introduction.

Furthermore, it was observed that the structural behavior changes with the size of the analyzed specimen. Also the link between acoustic emission parameters and the ultimate strength was shown experimentally, among others by Mpalaskas [4, 5], and this relation could be proposed for better understand the damage process in quasi-brittle materials.

[4] Mpalaskas AC, Matikas TE, Van Hemelrijck D, Papakitsos GS, Aggelis DG. Acoustic emission monitoring of granite under bending and shear loading. Archives of Civil and Mechanical Engineering. 2016, 16: 3, 313-324. https://doi.org/10.1016/j.acme.2016.01.006

[5] Mpalaskas AC, Thanasia OV, Matikas TE, Aggelis DG. Mechanical and fracture behavior of cement-based materials characterized by combined elastic wave approaches. Construction and Building Materials. 2014, 50, 649-656. https://doi.org/10.1016/j.conbuildmat.2013.10.022

8. Apart from comparing the final strength values between model and experiment, is it possible to compare also the cracking patterns? (E.g. branches of the cracks, point of crack initiation, extend of crack for specific load)

Yes, we have done several works where the ability of the LDEM when obtaining quantitative results is illustrated, see for example:

[30] Kosteski LE, Iturrioz I, Cisilino AP, Barrios D'ambra R, Pettarin V, Fasce L, Frontini P. A lattice discrete element method to model the falling-weight impact test of PMMA specimens. Int J Impact Eng. 2016, 87, 120-131. https://doi.org/10.1016/j.ijimpeng.2015.06.011

[46] Kosteski LE, Barrios D'Ambra R, Iturrioz I. Crack propagation in elastic solids using the truss-like discrete element method. I Int J Fract. 2012, 174, 139-161. https://doi.org/10.1007/s10704-012-9684-4.

9. Authors should try to enhance the practical side of the paper, how can this model be utilized?

The correlation between global behavior of the specimens, and the brittleness number (s) could be useful to define intervals of s where the specimens have a typical behavior of brittle-ductile transition. We consider that this aspect has been pointed out in the final conclusions of the paper. Moreover, the LDEM method was used to solve several problems in the field of Engineering. Examples of its applications were given in the last paragraphs of the introduction.

Highlights:

Carpinteri´s brittleness allows to identify specimen ductile-brittle global behavior.

Several experimental and numerical uniaxial tensile tests are done to verify the brittle number classification.

The use of this version of Lattice Element Method allows capturing the damage process in quasi-brittle materials.

This version of Lattice Element Method uses the brittleness number to calibrate the input parameters.

Size Effect in Heterogeneous Materials analyzed through a Lattice Discrete Element Method Approach

Luis Eduardo Kosteski[a], Ignacio Iturrioz[b], Giuseppe Lacidogna[c], Alberto Carpinteri[d]

[a] Associate Prof., Eng., Dr., PPEng, UNIPAMPA, Alegrete, RS, Brazil, luiskosteski@unipampa.edu.br.
[b] Full Prof., Eng., Dr., PROMEC, UFRGS, Porto Alegre, RS, Brazil, ignacio@mecanica.ufrgs.br
[c] Associate Prof., Arch., Dr., Department of Structural, Geotechnical and Building Engineering, Politecnico di Torino, Turin, Italy, giuseppe.lacidogna@polito.it
[d] Full Prof. Department of Structural, Geotechnical and Building Engineering, Politecnico di Torino, Turin, Italy, alberto.carpinteri@polito.it

Corresponding author´s e-mail: luiskosteski@unipampa.edu.br

Abstract

In the Lattice Discrete Element Method (LDEM), different types of mass are considered to be lumped at nodal points and linked by means of one-dimensional elements with arbitrary constitutive relations. In previous studies on the tensile fracture behavior of rock samples, it was verified that numerical predictions of fracture of non-homogeneous materials using LDEM models are feasible and yield results that are consistent with the experimental evidence available so far. In the present paper, a discussion of the results obtained with the LDEM is presented. A set of rock specimens of different sizes, subjected to monotonically increasing simple tensions, are simulated with LDEM. The results were analyzed from the perspective of the brittleness number, proposed by Alberto Carpinteri, to measure the brittleness level of the structure under study. The satisfactory correlation between the experimental results and LDEM results confirms the robustness of this method as a numerical tool to model fracture processes in quasi-brittle materials.

Keywords: Heterogeneous Materials, Lattice Discrete Element Method, Size Effect , Brittleness Number.

Nomenclature

A_i Cross-section area of the element to obtain the mechanical equivalence with the solid ($i=l$, longitudinal bars; $i=d$, diagonal bars).

A_i^* Cross section to obtain the fracture equivalence with the solid material.

b, D, d, r Dimensions that define the specimens' geometries.

d_{eq} Characteristic length of the material.

1   E, v Elastic constant: Young's modulus and Poisson's ratio, respectively.

2   ECL   Elemental Constitutive Law.

3   F Element axial force.

4     $F(t), P(t)$ Internal and external vector forces.

5   F_{max} The peak force measured in each bar.

6   G_f Fracture Energy

7   K_c The critical stress intensity factor.

8   L Length of the side of the cubic LDEM module.

9   L_{corr} The correlation length.

10   L_d Length of the diagonal elements.

11   LDEM   Lattice Discrete Element Method.

12   M, C Mass and damping matrices.

13   q The critical crack size.

14   R Structure characteristic length.

15   s, s_E Both version of the brittleness numbers proposed by Carpinteri

16   s_{LDEM} Brittleness number computed in the context of LDEM.

17   w Displacement.

18    $\ddot{x}, \dot{x}$ Nodal acceleration and velocity vectors.

19   Y The shape coefficient.

20   Z Specimen length or span.

21   Z/R The slender coefficient of the specimen.

22    $\delta_c, \delta_{50}, \delta_u$ Characteristic displacements measured in the LDEM global stress-

23   displacement responses.

24   ε_p Characteristic strain measured in each bar.

25   ε_r Failure strain measured in each bar.

26   ε_u Strain linked with σ_p.

27   ρ Specific mass.

28   σ Stress.

29   σ_p Global maximum strength

30   σ_p^* The stress that correspond with the ε_p

31    $\mu(.), CV(.)$ Mean value and variation coefficient.

32

1. Introduction

In the literature, the scale effects were extensively studied to connect the fracture process zone with the specimen size, the pioneer works of Dugdale [1], Boyle [2], and Brown and Srawley [3] could be cited among others. More specifically, in the so-called quasi-brittle materials, such as concrete, this topic was also widely discussed. This kind of materials are characterized by a disordered microstructure, exhibits damage localization, and are unable to present plastic or hardening deformations, having a non-negligible fracture process zone compared to the structure size. Furthermore, it was observed that the structural behavior changes with the size of the analyzed specimen. Also the link between acoustic emission parameters and the ultimate strength was shown experimentally, among others by Mpalaskas [4, 5], and this relation could be proposed for better understand the damage process in quasi-brittle materials.

Carpinteri [6-10] proposed dimensionless parameters: the brittleness numbers s and s_E, to measure the structural brittleness that describes the susceptibility of cracks to propagate in unstable conditions. These numbers are related to the change of behavior with the structural size and depend on the fracture energy and the yielding strength of the material as well as on the characteristic dimension of the structure:

$$s_E = \frac{G_f}{\sigma_p R}; \qquad s = \frac{K_c}{\sigma_p R^{1/2}} . \tag{1}$$

In these expressions, K_c is a measure of toughness, and G_f is a mechanical characteristic of brittle materials called fracture energy, following the nomenclature used by Carpinteri in his Cohesive Crack Model presented in [9, 11], σ_p represent the yielding or maximum stress, and R constitutes the characteristic structural dimension that defines the specimen's size. If we consider that $K_c = (G_f E)^{0.5}$ and $\sigma_p = E\varepsilon_u$, then the equivalence between the two adimensional numbers is:

$$s_E = s^2 \varepsilon_u, \tag{2}$$

where ε_u is the strain linked to σ_p.

Both nondimensional numbers have been used in several scientific papers in the last three decades [12-16, among others]. In Carpinteri [6, 7], the characteristics of these parameters are presented in detail, and the recommendation that s_E is more adequate to be used for brittle or quasi-brittle materials and s for ductile materials is highlighted. In the present work, the s instead of s_E parameter was used to measure the change of global behavior in the specimens that were tested and consequently simulated by the model.

1   The numerical simulations of structures made of quasi-brittle materials have the

2   implication that, in these materials, the characterization of the damage is often governed

3   by more than one single crack. The studies of a set of small fractures interacting at

4   different scale levels have great relevance when attempting to understand and simulate

5   the behavior of these materials. As mentioned by Krajcinovic [17], accounting for each

6   individual crack in the heterogeneous materials, assessing its influence on the structural

7   response and ultimately on the structural failure, is not a task that can be approached by

8   using conventional methods of analysis in solid mechanics. In this way, the methods,

9   which are able to represent naturally the discontinuities, could be an alternative method

10   of analysis. Among the non-conventional methods of continuous representation,

11   Peridynamics is widely used. Such method belongs to the family of Discrete Element

12   Methods. In this approach, the combination of nodes and associated discrete mass by

13   means of an interaction law applied between neighbor nodes represents the continuum.

14   The proposal carried out for the Peridynamics was used originally to represent the

15   interaction force at the atomic level. Seleson [18] could be cited here as an example of

16   this approach. Moreover, the same approach was also applied at large scale levels, all

17   thanks to the pioneering work by Silling [19].

18   Another equivalent discrete approach is the Truss-like Discrete Element Method

19   or Lattice Model. Various and relevant approaches study can be referred to; among others

20   like the ones proposed by Schlangen and van Mier [20], Krajcinovic and Vujosevic [21],

21   and, more recently, the works of Sagar and Prasad [22], Nagy *et al.* [23], and Rinaldi [24].

22   A review of the different versions of Discrete Element Method, including the Particle

23   methods and Lattice approaches, is presented in Mastilovic and Rinaldi [25].

24   In the present paper, a version of the Lattice Discrete Element Method (LDEM)

25   proposed by Riera [26] will be used. This method was developed originally to determine

26   the dynamic response of plates and shells when failure occurs primarily by shear or

27   tension under a shock wave caused by impact loading, as it is generally observed in

28   concrete structures.

29   In the LDEM, the quantities of mass are considered lumped at nodal points and

30   linked by means of one-dimensional elements with arbitrary constitutive relations. The

31   satisfactory correlation between the experimental results and the LDEM predictions

32   confirms the robustness of this method as a numerical tool to model fracture processes in

33   quasi-brittle materials. These findings were reported, among others, in a successful

34   analysis of: shells subjected to impulsive loading [27-30], the fracture of elastic

1 foundations on soft sand beds [31], the generation and propagation of an earthquake [32-
2 35], the study of the scale effect in quasi-brittle materials [36-42]; the computation of
3 fracture parameters in static and dynamic problems [43-46], the study of strength of brittle
4 materials under high strain rates [47] and finally the acoustic emission events in quasi-
5 brittle materials [34, 35, 48-50]. In Refs. [29-31, 36, 46, 51], LDEM simulations were
6 discussed in which quantitative comparison with experimental results in terms of global
7 parameters, such as displacement versus loads or final configurations, are presented. The
8 following section presents a brief description of the theoretical foundation of this method.
9
10 **2. Lattice Discrete Element Method Formulation**
11   The Lattice Discrete Element Method (LDEM), used in the present work,
12 represents the continuum by means of a 3D lattice, that is, a periodic spatial arrangement
13 of bars with amounts of mass lumped at their ends. Figure 1 shows the discretization
14 strategy in which the stiffness of the LDEM elements, corresponding to an equivalent
15 orthotropic linear elastic material, was obtained by Nayfeh and Hefzy [52]. The basic
16 cubic module is built with twenty bars and nine nodes. Each node presents three degrees
17 of freedom given by the spatial components of the displacement vector in the global
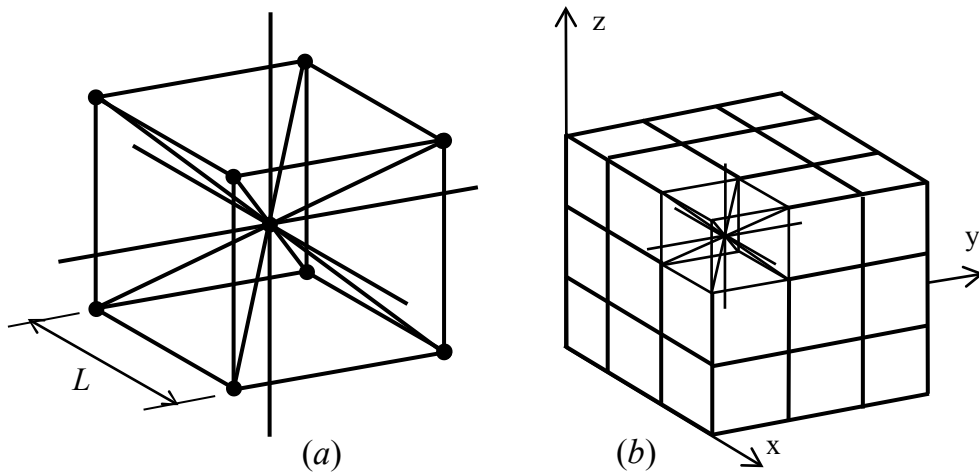18 reference system.

19
20 Figure 1- LDEM discretization strategy: (a) basic cubic module, (b) generation of the
21   prismatic body.
22

23   In case of an isotropic elastic material, the cross-sectional area A_l of the
24 longitudinal elements (those defining the edges of the module and those that are parallel
25 to the edges connected to the node located at the center of the module) in the equivalent
26 discrete model is:

5

1          $A_l = \phi L^2,$ (3)

2 where L is the length of the side of the cubic module under consideration. The function

3 $\phi = (9 + 8\delta)/(18 + 24\delta)$, where $\delta = 9\nu/(4 - 8\nu)$ accounts for the effect of the

4 Poisson's ratio ν [49, 30]. Similarly, the area A_d of the diagonal elements is:

5          $A_d = \phi L_d{}^2 = \frac{2}{\sqrt{3}}\delta\phi L^2,$ (4)

6 were $L_d = \frac{2}{\sqrt{3}}L$ is the length of the diagonal elements. The coefficient $2/\sqrt{3}$ in Eq. (4)

7 accounts for the difference in length between the longitudinal and the diagonal elements.

8   It is important to point out that, for $\nu = 0.25$, the correspondence between the

9 equivalent discrete solid and the isotropic continuum is complete. On the other hand, for

10 values of $\nu \neq 0.25$ discrepancies appear in the shear terms. These discrepancies are small

11 and may be neglected in the range $0.20 \leq \nu \leq 0.30$. For values of ν outside this range, a

12 different basic module should be used (see Ref. [52]). It is interesting to note that while

13 no lattice model can exactly represent a locally isotropic continuum, it can also be argued

14 that no perfect locally isotropic continuum exists in the physical world. Isotropy in solids

15 is a bulk property that reflects the random distribution of the orientation of constituent

16 elements. A comprehensive study on the effect of the LDEM lattice geometry on the value

17 of the Poisson's ratio can be found in Ref. [53].

18   The equations of motion are obtained from equilibrium conditions of all forces

19 acting on the nodal mass, resulting in a system of equations of the form:

20          $M\ddot{x} + C\dot{x} + F(t) - P(t) = 0,$ (5)

21   where $\ddot{x}$ and $\dot{x}$ are, respectively, the nodal acceleration and velocity vectors; M

22 and C are the mass and damping matrices, respectively, and the vectors $F(t)$ and $P(t)$

23 convey the nodal internal and external forces. Since M and C are diagonal, the equations

24 in Eq. (5) are not coupled, and they can be easily integrated in the time domain using an

25 explicit finite difference scheme.

26   It is worth noting that, since the nodal coordinates are updated at each time step,

27 large displacements are accounted for naturally. The convergence of LDEM solutions in

28 linear elasticity and elastic instability problems was verified by [32], among others.

29   The irreversible effects of crack nucleation and propagation that occur in brittle

30 or quasi-brittle materials were taken into account by [54], and more recently by [45],

31 through the introduction of a non-linear constitutive model that reduces the element load

1 carrying capacity. More details of this implementation can be found in [43-46, 54], among

2 others.

3   Based on Hillerborg's theory [55], the bilinear model for quasi-brittle materials

4 used in this work is shown in Figure 2. In case of tensile loads, the area under the force -

5 strain curve (the area of the *OAB* triangle in Figure 2) is the energy density necessary to

6 fracture the area of element influence, the fracture energy. Thus, for a given point *P* on

7 the force - strain curve, the area of the *OPC* triangle represents the reversible elastic

8 energy density stored in the element, while the area of the *OAP* triangle is the dissipated

9 fracture energy density. One element fails and loses its load carrying capacity when the

10 dissipated energy density equals the fracture energy.
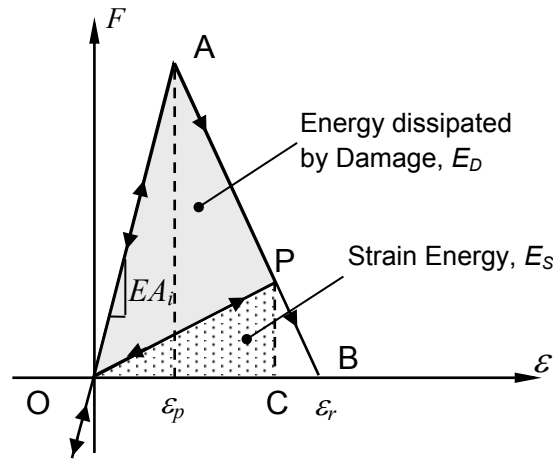

12 Figure 2: Bilinear constitutive model with material damage.

14   In the case of compressive loads, the material behaves in a linear elastic manner.

15 In this way, the failure in the compression is induced by indirect traction. In quasi-brittle

16 materials, this assumption is reasonable because its ultimate strength in compression is

17 usually five to ten times larger than that in tension [56].

18   In the constitutive model presented in Figure 2, *F* is the element axial force, and

19 A_i the cross-section area of the element, depending whether longitudinal or diagonal

20 element is considered, as in Eq. (3) and Eq. (4). In this model, the fracture energy per unit

21 area coincides with the material fracture energy, G_f.

22   The so called critical strain $\varepsilon_{p,}$ as illustrated in Figure 2, is the maximum strain

23 before damage initiation. The critical strain is a micro-parameter, that is, a parameter that

24 governs the constitutive law at the elemental level. The *limit strain* ε_r is the strain value

25 for which the elements lose its load carrying capacity (point B in Figure 2). The limit

26 strain is much greater than or equal to the critical strain. This value is calculated to satisfy

the fact that the dissipated energy density released when the element fail must be equal to the multiplication of the equivalent fracture area of the element, A_i^*, times the fracture energy, G_f, divided by the element length, L, that is:

$$\int_0^{\varepsilon_r} F(\varepsilon)d\varepsilon = \frac{G_f A_i^*}{L_i}. \tag{6}$$

The index i in the expression indicates it either refers to longitudinal or the diagonal elements.

The area below the bilinear model is $\varepsilon_r \varepsilon_p E A_i / 2$, then, the final strain defined for the element ε_r, illustrated in the Figure 2, is designated as:

$$\varepsilon_r = \frac{G_f}{\varepsilon_p E}\left(\frac{A_i^*}{A_i}\right)\left(\frac{2}{L_i}\right), \tag{7}$$

A_i^* denotes the equivalent fracture area of each element defined in order to satisfy the condition that the energy dissipated by the fracture of the continuum and by its discrete representation are equal, $A_i^* = \frac{3}{22} L_i^2$. This deduction can be found in [45]. It should be noted that ε_r depends on the material properties and on the level of discretization.

Young's modulus E, the stress intensity factor K_c and the critical stress σ_p are related by the classical fracture mechanic expression [57] given below:

$$K_c = \sigma_p Y \sqrt{\pi q}, \tag{8}$$

in which Y is a parameter that accounts for the influence of the boundary conditions and the orientation of the critical crack size q. If it is assumed that the behavior up to the beginning of the rupture is linear, then $\sigma_p^* = E\varepsilon_p$ and, recalling the equivalence between K_c and the fracture energy G_f, we obtain the expression:

$$\sqrt{G_f E} = E\varepsilon_p Y \sqrt{\pi q}. \tag{9}$$

This assumption is very important for this development because the tension obtained ($\sigma_p^* = E\varepsilon_p$) is not the global maximum strength σ_p, as defined in Eq. (1), but instead, is a local or elemental maximum.

In order to simplify Eq. (9), an equivalent length d_{eq} is defined as follows:

$$d_{eq} = q\pi Y^2. \tag{10}$$

Substituting Eq. (9) in (10), then:

$$d_{eq} = \frac{G_f}{(\varepsilon_p)^2 E} \tag{11}$$

Eq. (11) indicates that d_{eq} may be regarded as a material property, since it does not depend on the discretization level, representing in fact a *characteristic length of the*

1 *material* (similar as the width of the plasticity region in the crack tip in the Dugdale
2 model).

3   It also is possible to isolate ε_p from the Eq. (11) to obtain:

4 $$\varepsilon_p = \sqrt{\frac{G_f}{d_{eq}E}},$$ (12)

5 and replacing (11) in ε_r Eq. (7) it is found:

6 $$\varepsilon_r = \varepsilon_p d_{eq}\left(\frac{A^*_i}{A_i}\right)\left(\frac{2}{L_i}\right),$$ (13)

7 Eq. (12) shows that maintaining E and G_f constant, when the d_{eq} increases, a more ductile
8 behavior is expected. The area below the elemental constitutive relation (see Fig. 2) is
9 linked to G_f, then, if this parameter remains constant, the decrease of ε_p has to be
10 compensated by increasing the value of ε_r to maintain the area below the curve.

11   When ε_p is equal to ε_r, the minimum area of bilinear constitutive model is
12 obtained, that is, the limit relation between the equivalent length and the element length,
13 for longitudinal elements, is found to be $d_{eq} \geq \frac{15}{22}L$. In some way, from the Eq. (13) it is
14 possible to say that $\varepsilon_r/\varepsilon_p \propto d_{eq}/L$, that is, d_{eq}/L is related to the bilinear constitutive
15 model. If the constitutive model is "brittle" (ε_r next to ε_p), d_{eq}/L will be small, however,
16 if the constitutive model is "ductile" (ε_r much larger than ε_p) d_{eq}/L will be higher.

17   It can be noticed that a characteristic length as material parameter is also discussed
18 in another version of the discrete element method called Peridynamics, proposed by
19 Silling *et al.* [58]. In this method, there is a set of nodes where the mass are discretized
20 and linked with bars, moreover, the level of neighboring among nodes is given by a
21 material parameter called horizon. This parameter depends on the discretization level
22 used to define the quantity of nodes linked to one and another. The horizon physical
23 meaning is analogous to the meaning of the d_{eq} in the version of the Discrete Element
24 Method used in the present work.

25   Taylor [59] considers that a breaking criterion is fulfilled when a dominium
26 portion, defined by a characteristic dimension, reaches the critical level of stress. In this
27 approach, both parameters are considered as material parameters. The link between the
28 characteristic distance of this author and the d_{eq} is evident.

29   The randomness of the model is introduced considering G_f as a random field with a
30 Weibull density function characterized by its mean value $\mu(G_f)$ and variation coefficient

$CV(G_f)$. Moreover, it is necessary to consider the spatial correlation function of this random parameter. How to consider the random nature in the model could be explained in [30, 60].

In the model here implemented, the random values of G_f assigned to every element have statistical independence, that is, the random properties of one element do not depend on the properties of the other neighboring elements. This assumption is equivalent to consider that the correlation length is $L_{corr} = 0.3L$. Notice that when randomness is introduced in G_f, indirectly randomness is also introduced in ε_p (see Eq. 12). In this way, the maximum strength of an element $F_{max} = EA_i\varepsilon_p$, which is directly related to point A in Figure 2, is also random. The axial stress of the element will be: $\sigma_p^* = E\varepsilon_p$. Another alternative to introduce the random nature in the model is to consider geometric perturbation in the mesh, about this aspect see [61]. More detail about the LDEM formulation can be found in Ref. [50].

Below, several points are explained to clarify the meaning of the parameters used in the definition for the constitutive law of the LDEM model:

(i) The concept of the brittleness number s in the context of LDEM is introduced with the aim of showing evidence of the physical meaning of the parameter d_{eq} previously defined.

If we rewrite the Eq. (1) that introduces the *brittleness number s* proposed by Carpinteri [6], we consider that $\sigma_p = \sigma_p^*$ and recalling the equivalence between K_c and the fracture energy G_f, the expression of s in the context of the LDEM formulation will be:

$$s_{LDEM} = \frac{K_c}{\sigma_p^* R^{1/2}} = \frac{\sqrt{G_f E}}{E\varepsilon_p R^{1/2}} = \sqrt{\frac{d_{eq}}{R}}. \tag{14}$$

From this expression it can be interpreted that, if a crack of a size $> d_{eq}$ appears during the damage process in a structure with a characteristic dimension R, it will propagate in an unstable form, suggesting a brittle global structural behavior. However, this situation will only be possible if d_{eq} is lower than R. If this condition is not fulfilled, it will not be possible to have a crack with a dimension similar to d_{eq}, because there is not enough space in the structure for crack propagation. In the latter situation, the structure will have a ductile behavior during its damage process. The structure boundary condition influences this relation but it does not change the general tendency.

The ratio between Eq. (1) and (14) allows writing the relationship between the traditional expression of the brittleness s with its definition in the context of LDEM. As it was previously emphasized, the difference resides in the definition of σ_p: in the classical expression of s, σ_p is the stress value in which the material collapses, while in the s_{LDEM} definition, $\sigma_p = \sigma_p^*$ is the axial stress of the elements. The ratio s/s_{LDEM} is a function of the statistical and spatial distribution of the random field that characterizes G_f, and the shape of the elemental constitutive law used. At the end of the present work, a further comment about this ratio is provided.

(ii) In contrast to the usual practice used in the Finite Element Method, the constitutive relationship in the LDEM is not only a function of the material properties. The LDEM model considers the following macroscopic parameters: the elastic modulus E, the fracture energy G_f, and the characteristic length d_{eq}. With these three parameters using Eq. (12), the critical strain ε_p, where the bar force reaches its maximum value is computed (see Fig 2). Multiplying E by the Eq. (3) and (4) the linear pre-peak relation in the elemental constitutive law (ECL), defined by EA_i, is indicated in Figure 2. The fracture energy G_f directly influences in the area below the ECL, as it is indicated in Eq. (6). Furthermore, using Eq. (13) as illustrated in Fig. 2, the characteristic length of the material, d_{eq}, defines the post-peak branch in the ECL by means of the local parameter ε_r. Notice that not only ε_r, but also EA_i depend on the discretization level.

(iii) Another interesting feature of the method is that, although it uses a scalar damage law to describe the uniaxial behavior of the elements, involves a global model that takes into account of the anisotropic damage. This is because, when the uniaxial bars, oriented in different directions, are damaged they modify their axial stiffness, allowing to represent an anisotropic global behavior.
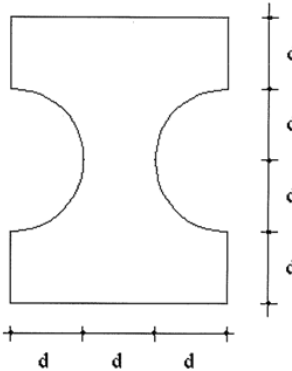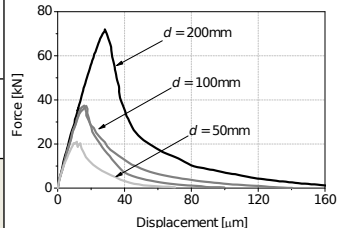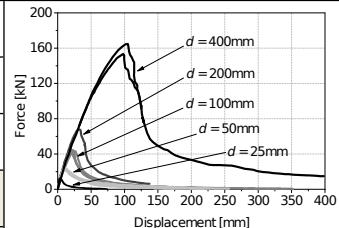
3. Experimental background

The results obtained by Carpinteri and Ferro [62, 63], van Vliet [64] as well as van Vliet and van Mier [65], all of whom have studied the scale effects on tensile strength of concrete and rock, are used to explore the link between the brittleness number, s, proposed by Carpinteri [6, 7] and the global behavior obtained in the cited cases that could be classified as ductile or brittle. Experimental results obtained by the authors over expanded polystyrene samples are also described and analyzed.

1 **3.1 Carpinteri and Ferro Results**

2   Carpinteri and Ferro [62, 63] and Carpinteri and Maradei [65] carried out two sets

3 of tests with specimens of several sizes. The Young's Modulus was measured from the

4 global stress versus strain curves, at around 35GPa for the two sets. The material

5 parameters and the brittleness number values s, computed using Eq. (1), are presented in

6 Table 1. The characteristic dimension R was considered in the present case as the

7 dimension of the specimen neck, d.

8   In both series, the specimen with characteristic size d smaller than 100 mm

9 showed a ductile behavior, whereas specimens with d larger than 200 mm showed a

10 quasi-brittle behavior. In both sets of results s <1.4 indicates a quasi-brittle global

11 behavior

12

13 Table 1: Material parameters, the brittleness number computed and the curves used as
14   sources of information for the experimental sets 1 and 2 presented by Carpinteri and
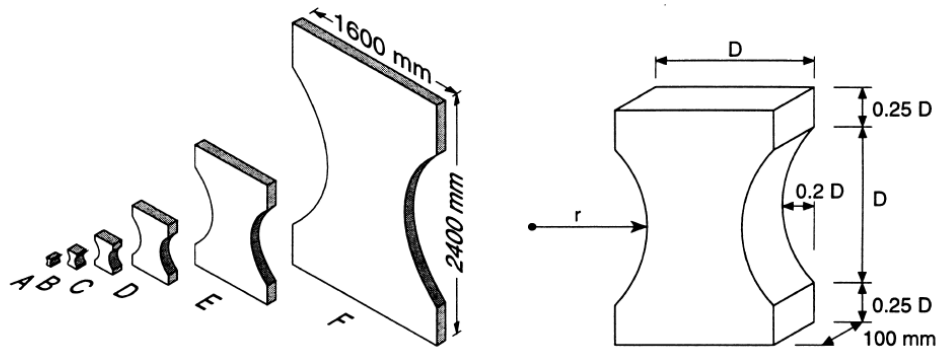15   Ferro [62, 63]. (E=35 GPa).

d [mm]	σ_p [MPa]	G_f [N/m]	s	Experimental Results	Specimen Geometry
Set 1					
50	4.25	83	1.79		
100	3.78	102	1.58		
200	3.64	142	1.37		
Set 2					
25	4.79	147	2.99		
50	4.56	257	2.94		
100	4.37	236	2.08		
200	3.80	158	1.38		
400	3.72	286	1.34		

16

17

18 **3.2 van Vliet and van Mier's Results**

19   van Vliet [64] performed three sets of tests of specimens using different

20 dimensions, as is shown in Fig. 3. The first set was conducted by using concrete stored in

21 the laboratory in a dry environment, called the DRY set. The second set also was with

1   concrete, however stored in a climate room, called the WET series. Finally, the third set

2   of specimens consists of Felser sandstone specimens called FELSER.

3   For the calculus of the brittle number, the fracture energy G_f measured

4   extrapolating the stress opening curve (σ-w) was used. The material parameters and the s

5   values computed are presented in Table 2. In the present cases, the characteristic

6   dimension R to compute the brittleness number s with the Eq. (1) is $0.6D$, the specimen

7   neck, as could be appreciated in Fig 3.

8

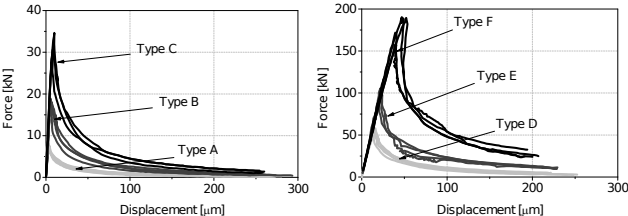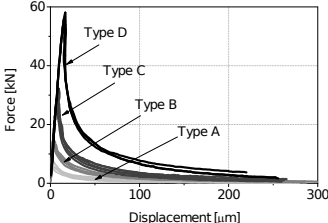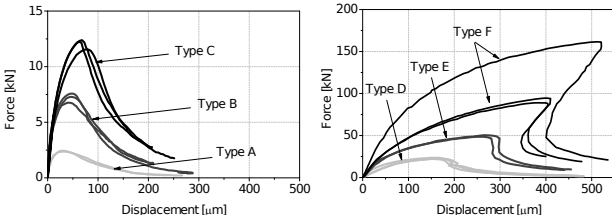| Type	A	B	C	D	E	F
D [mm]	50	100	200	400	800	1600
r [mm]	36.25	72.5	145	290	580	1160

10   Figure 3. Specimen shape and dimensions for van Vliet [64] adopted size range.

11

12   For all the van Vliet experiments, represented in Table 2, it is possible to observe

13   an apparent change in the global behavior for specimen with brittle number s near to 1.5.

14   For s values lower than 1.6, specimen F ($s = 1.34$) for the DRY set, specimen D ($s = 1.57$)

15   for the Wet set and specimens D ($s = 1.48$), E ($s = 1.07$) and F ($s = 0.74$) for the FELSER

16   set, the global response seems to be brittle. Finally, for s values higher than 1.6, a clearly

17   ductile global response is observed.

18   In fact, it is possible to consider that with s between 2 to 1 we are in a transition

19   zone, and a very clear brittle behavior could be defined when s is lower than 1, as seen

20   for the F($s = 0.74$) specimen in the FELSER set.

21

Table 2: Material parameters and brittleness number computed for the van Vliet [64] specimens.

Type	σ_p [MPa]	G_f [N/m]	E [GPa]	s	
DRY set					
A	2.54	97.0	88.42	6.66	
B	2.97	125.7	38.5	3.02	
C	2,75	124.2	39.41	2.32	
D	2.30	125.2	42.80	2.05	
E	2.07	142.3	38.25	1.63	
F	1.86	141.1	42.55	1.34	
WET set					
A	2.17	91.1	40.48	5.11	
B	2.23	99.6	39.80	3.64	
C	2.48	88.9	42.38	2.26	
D	2.37	100.4	33.25	1.57	
FELSER sandstone set					
A	0.82	76.7	4.75	4.25	
B	1.22	111.3	7.90	3.14	
C	1.01	93.8	6.87	2.29	
D	0.96	135.1	3.60	1.48	
E	1.30	143.9	6.50	1.07	
F	1.20	93.2	8.23	0.74	

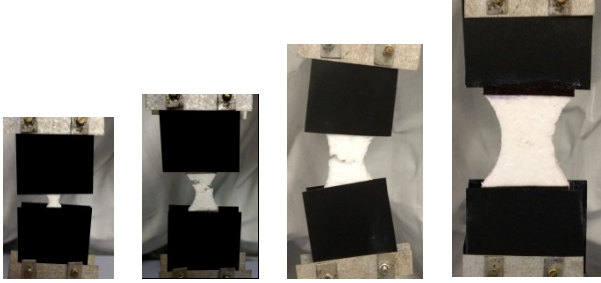**3.3 Expanded polystyrene experimental results**

In the following section, a set of tests carried out by the authors on expanded polystyrene are presented. The material was submitted to direct tensile stress using specimens with the same geometry, but different sizes compared to the ones used by Van Vliet [64]. The tests were carried out in a Universal Machine Test Shimadzu AGS - X 5 kN in the Federal University of Pampa - Brazil.

In Table 3 the dimensions of the body tests called A, B, C and D are presented. Four tests were conducted for each configuration. For all the four specimen geometries, the thickness was always 9 mm. The specimens were fixed at the ends, as illustrated in

1 Table 3 by applying the prescribed displacement at the top end at a constant displacement

2 rate of 0.0333 mm/min.
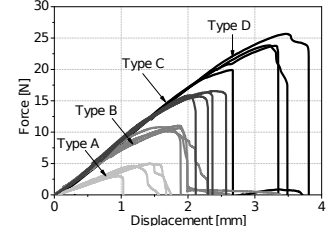
3

4

Table 3. Body test dimensions.

Type	A	B	C	D
D [mm]	10	20	30	45
r [mm]	7.25	14.5	21.75	32.63

5

6   Fracture energy G_f equal to 25N/m, value also adopted by Colpo *et al.* [42], was

7 used for the calculus of the brittleness number by using Eq. (1). These results are

8 presented in Table 4. As done in previous tests, the specimen characteristic length R was

9 considered to be equal to the neck specimen, $0.6D$.

10   A similar tendency, to what was observed in previous cases, was also appreciated

11 in the results obtained using expanded polystyrene. When the s value is lower than 1, the

12 global stress curve clearly shows a brittle behavior, and when the results of s are between

13 the interval 2.0 to 1.0, a transition behavior is observed.

14

15 Table 4: The brittleness number computed for the set of test carried out over expanded
16   polystyrene specimens.

Type	σ_p [MPa]	CV [%]	E [N/mm²]	CV [%]	s	
A	0.049	21.4	0.89	12.1	1.24	
B	0.059	3.4	1.73	8.4	1.02	
C	0.060	2.5	2.01	12.8	0.88	
D	0.058	10.4	2.21	9.3	0.78	

17

18   With the aim of categorizing the global behaviors in all the tests carried out, a

19 typical brittle global response it is considered when:

a) considering tests under controlled displacement, after reaching the peak load, the global displacement is smaller than that corresponding to the peak load. As in the case of the (F) specimens of the FELSER sandstone set presented in Table 2;

b) considering tests under force control, after reaching the peak load, the behavior is characterized by a clear jump in the load, without any significant softening branch. The specimen (D), presented in Table 4, is an example of this second case.

On the other hand, a typical ductile global behavior is considered when the global post-peak displacement is higher displacement corresponding to the peak load. The Felser tests from (A) to (C), presented in Table 2, are clear examples of this kind of global behavior.

When it is not possible to define a clear brittle, or ductile behavior, we consider this case as a global transition behavior, see, for example, specimen (A) of the Polystyrene specimens presented in Table 4.

It is important to highlight here that, in Carpinteri [6, 7], the author reaches the conclusion that, for specimens subjected to tension or compression, the following equation

$$\frac{s_E}{\left(\frac{Z}{R}\right)\varepsilon_u} \leq \frac{1}{2}, \tag{15}$$

defines the condition for Snap-Back instability that governs the global mechanical behavior. In the Eq. (15), Z is the specimen length or span and Z/R represents the slenderness. For the cases studied in the present work, Z/R is always considered close to 1. Remembering the equivalence given between s_E and s presented in Eq. (2), Eq. (15) could be rewritten in terms of s as $s^2 \leq 1/2$, i.e. $s \leq 1/\sqrt{2} \sim 0.7$, a result that could be considered as a lower bound for the numerical results presented in the following section.

However, in the three experimental results presented, the shape of the specimens considered is not prismatic. Therefore, the difference in shape could explain that, in the described conditions, the transition to the brittle behavior seems to be defined by $s \leq 1$ instead of $s \leq 0.7$. The extension of the present study with the aim of verifying the influence of the slenderness, other geometric characteristics as well as other boundary conditions will be the focus of future works.

1 **4 LDEM simulations: rock specimens with different sizes subjected to uniaxial**

2 **tensile stress**

3 **4.1 Model description**

4   A specimen group of heterogeneous material was simulated being fixed at their

5 lower face and subjected to monotonically increasing displacements at the nodes on their

6 upper faces. In all cases, nodal displacements in the normal direction to the middle surface

7 were restrained in order to simulate plane strain conditions. The specimens were analyzed

8 up to the complete failure. The specimen side b ranges between an interval of 0.05 and

9 3.50m. The smallest LDEM array that leads to satisfactory results consists of 10×10×1

10 cubic modules with 1026 DOF which were used for the smallest (0.05m) model. Whereas

11 the 3.50m model consists of 700×700×1 cubic modules with 1472802 DOF, thus,

12 constituting the largest specimen used in this study. Table 5 shows the basic dimensions

13 of the samples, while Table 6 indicates the relevant material properties.

14

15   Table 5: The dimensions of the LDEM models studied.

Specimen	1	2	3	4	5	6	7	8	9	10	11	12	13
b (m)	0.05	0.075	0.10	0.15	0.20	0.25	0.30	0.40	0.50	0.75	1.00	1.50	3.50
Cells	10	15	20	30	40	50	60	80	100	150	200	300	700

16

17   Table 6: Relevant rock (granite) material properties and LDEM parameters.

Material Properties	Value
E (Young's modulus)	75 GPa
ρ (specific mass)	2700 kg/m^3
ν (Poisson coefficient)	0.25
LDEM Properties	**Value**
L (basic modulus length)	0.005 m
d_{eq}	1.465 m
$\mu(G_f)$ (Expected value of fracture energy)	1300 N/m
CV(G_f) (coefficient of variation of G_f)	40%

$\varepsilon p = 1.0878 \times 10^{-4}$

$\varepsilon r = 2.207 \times 10^{-2}$

It is important to note that in the simulations, the expected value of the fracture energy, $\mu(G_f)$, was considered as a mean value for all the sizes being simulated, instead of considering it as a variable with the size scale.

The layout of the specimens showing their relative size and boundary conditions is shown in Figure 4. It should be noticed that the fracture energy G_f is modelled as a random field using the properties indicated in Table 6. The probability distribution of G_f was considered as a Weibull function with a correlation length equal to $L_{corr} = 0.3L$, which is related to the material microstructure. As the material properties are associated with a statistical distribution, each simulation leads to a different strength and a different stress-strain curve. For this reason, four simulations were carried out for each size specimen in order to obtain representative results for each size specimen. As explained before, the correlation length used in this work is small, then the random values of G_f assigned to every bar are statistically independent, that is, the properties of one bar do not depend on the properties of the neighbor ones.

Figure 4. Relative size of the specimens and boundary conditions considered.

4.2 Results

One representative sample of the final simulated configuration for each size considered in the study is shown in Figure 5, in which the colors cyan, orange, and red represent undamaged, damaged, and totally broken (failed) elements, respectively. The sizes of the specimens are indicated in Figure 4.

The influence of the mesh discretization is studied in Refs. [46, 60], moreover, in the simulations presented here, the discretization level is similar. In addition, in Ref. [67]

1   was verified that the influence of the mesh rotation is marginal (less than 5%) in terms of

2   global results and fracture configurations.

3

| b=0.05m | b=0.075m | b=0.10 | b=0.15m | b=0.20m |

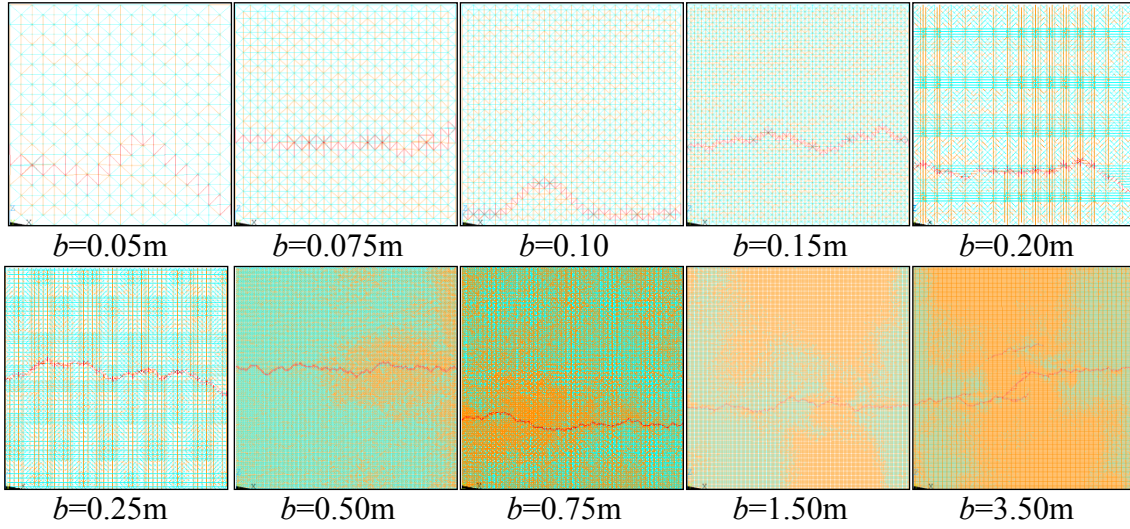| b=0.25m | b=0.50m | b=0.75m | b=1.50m | b=3.50m |

4

5   Figure 5. Damage distribution and rupture configuration of specimens of various sizes

6   subjected to applied displacements inducing uniaxial tension. The characteristic

7   specimen size b varies between 0.05 m and 3.5 m. The broken bars are indicated in red,

8   the damaged bars in orange and the undamaged bars in cyan.

9

10   The resulting stress displacement curves for all simulations of the b=0.20m

11   specimens, as well as the average curve, are shown in Figure 6. In this figure, the main

12   parameters that characterize the stress displacement curves are represented, in which σ_p

13   denotes the ultimate or maximum global stress, δ_c represents the critical displacement, or

14   displacement related to ultimate stress, and δ_u represents the ultimate displacement or the

15   displacement at the point where the strength is totally exhausted which has been defined

16   for practical purposes as the displacement when the stress decreases below 2% of the

17   maximum stress, σ_p. This notation is applicable without any restriction to specimens with

18   sides smaller than 0.4m. For specimens with b equal to 0.4m or larger, failure occurs in a

19   brittle manner and the ultimate displacement δ_u cannot be distinguished from the critical

20   displacement δ_c. Figure 6 also shows the displacement defined as δ_{50}, that is, the

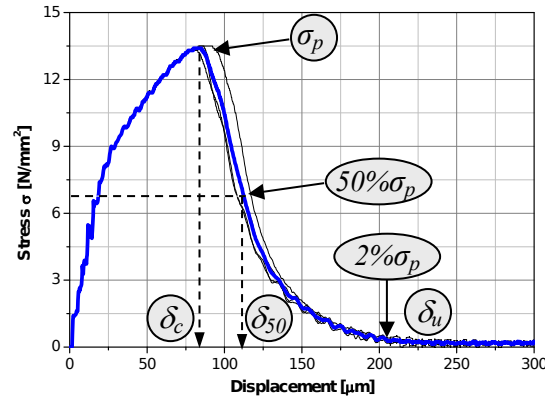21   displacement related to 50% of the rupture stress.

Figure 6. Curves for the mean vertical stress at lower support versus mean displacement for the b=0.20m rock specimen obtained from four simulations (black) and the average curve ones (blue).

In Figure 7(a) the global displacement versus mean stress curve for all the sizes simulated with LDEM are shown. In Fig. 7(b) the same results are presented considering the global displacement in a Log scale. In these figures, it is possible to see how the curves trend changes: specimens smaller than 0.25 m show a ductile behavior (black lines), specimens larger than 0.75 m present a brittle behavior (gray lines), whereas specimen sizes between 0.25 and 0.75 m show a transition between ductile and brittle behavior (red lines).

Figure 7. a) Displacement versus stress and b) log displacement versus stress curves for different size specimens. Ductile behavior when b<0.25 (black curves), brittle behavior when b>0.75m (gray curves), transition ductile-to- brittle behavior when b belongs to the interval [0.25, 0.75] (red curves).

1   The simulations resulted in different fracture patterns that in some cases produced
2   one, two or more cracks. It is worth noticing that the auto-similar configuration was used
3   throughout this work. For this reason, simulations, in which only one macro-crack
4   propagate, were considered. As it can be seen in Figure 5, b = 3.5m, there is more than
5   one crack in the final configuration, but the other cracks or its bifurcation become stable
6   and do not propagate to broke the specimen. When more than one crack propagates, the
7   stress-strain curves present a different morphology.

8   As shown in Figure 6, it is possible to specify the stress - displacement curves
9   through characteristic values without losing essential information. Table 7 lists the
10   correspondent characteristic mean values of the stress-displacement curves by increasing
11   the specimens' size.

12   Table 7 also presents the Carpinteri's brittleness number s obtained by Eq. (1),
13   assuming that $R = b$ the size of the specimen, and E and G_f the simulations parameters
14   presented in Table 6.

15

16   Table 7 – Mean values of peak stress, critical and rupture displacement of different
17   simulated specimen size.

b [mm]	σ_p [MPa]	CV [%]	δ_c [µm]	CV [%]	δ_u [µm]	CV [%]	δ_{50} [µm]	s Eq. (1)	s_{LDEM} Eq. (14)
50	13.461	1.10	26	7.42	225	4.53	93	3.26	5.41
75	13.518	0.85	34	7.30	211	5.01	89	2.67	4.42
100	13.415	0.98	43	5.63	207	4.08	94	2.33	3.83
150	13.508	0.63	64	0.04	213	0.14	103	1.90	3.12
200	13.473	0.39	85	3.13	213	2.44	110	1.64	2.71
250	13.429	0.68	105	1.31	203	1.76	126	1.46	2.42
300	13.393	0.16	124	0.15	185	4.77	132	1.35	2.21
400	13.488	0.31	166	1.29	184	3.33	176	1.16	1.91
500	13.471	0.30	205	1.36	228	2.41	216	1.04	1.71
750	13.455	0.39	301	1.92	322	1.72	301	0.85	1.40
1000	13.420	0.20	397	1.24	420	1.20	397	0.74	1.21
1500	13.437	0.20	605	0.76	646	0.76	605	0.60	0.99
3500	13.347	0.21	1325	1.87	1444	0.60	1325	0.39	0.65

18

19   By comparing the stress-displacement curves presented in Figure 7, it is possible to
20   identify two limits, i.e., brittleness numbers that define changes in the specimen behavior:
21   $s_{ub} \cong 1.5$ (upper bound), and $s_{lb} \cong 0.7$ (lower bound). Ductile behavior is expected for
22   $s > s_{ub}$, brittle behavior for $s_{lb} < 0.7$, and transitional behavior when $s_{lb} < s < s_{ub}$.

23   The experimental and numerical results in terms of the brittleness number s, and
24   global behavior (brittle-ductile transition), are shown in Figure 8. A global brittle
25   behavior is considered if s is smaller than 0.7, a ductile one if s is higher than 1.5. A

transition can be considered if s is comprised in the interval [0.7, 1.5]. It should be noted that $s < 0.7$ is a lower bound, but tests with brittle global behavior can occur with values above this limit. Furthermore, the ductile transition limit $s > 1.5$ shows a certain level of dispersion. The specimen shape and the influence of boundary conditions could be responsible for this dispersion. But despite this behavior, the limits $s<0.7$ and $s>1.5$ identify that the typical brittle-ductile transition take place in the specimens.

Figure 8: Representation of the s values in experimental and numerical results.

In Figure 9(a), the size effect in the mean ultimate stress is presented, and in Figure 9(b) the mean critical and ultimate displacement is also plotted. In both cases, the log scales are used to facilitate the result interpretation. A bar with +/- 2 standard deviation is included in the plots and between this bar 95% of the values obtained in the simulation are contained.

In Fig. 9(a), it is clear that the size effect in the global ultimate stress is practically null. This effect could be seen in the values presented in Table 7. The difference between the maximum and minimum values of mean global stress is 1.23% and the variation coefficients do not exceed 1.64%. The sensitivity of the global parameters with the size effect depends on several factors, such as the boundary conditions, and the random nature of the material input data. In Rios and Riera [36] experimental tests with different geometries and boundary conditions were simulated with LDEM, and the values of strength and its variability are reached with success.
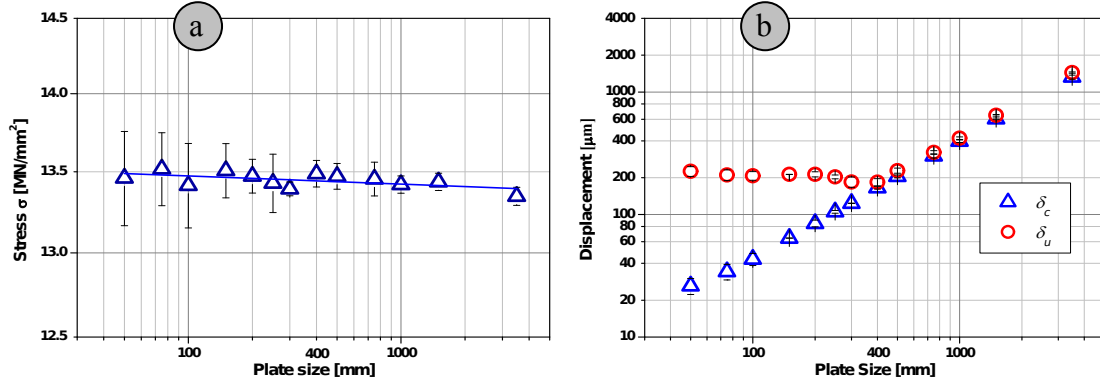
Figure 9. (a) Ultimate global stress. (b) Ultimate and characteristic global displacement versus the specimen dimension. The mean values and bar with +/- 2 standard deviation are indicated in the figure.

On the other hand, in Fig. 9(b) the specimen behavior changes in shape clearly for b =0.4 m; this result is compatible with the limits indicated in Fig. 7 and in Table 7.

A new parameter was defined to take into account the shape of the global stress versus displacement curve, or force versus displacement. The parameter proposed was the ratio δ_{50}/δ_c, between the displacement δ_{50}, when 50% of the rupture stress was reached, over the displacement δ_c, when the ultimate stress occurred. Thus, when a value of δ_{50}/δ_c is close to 1.0, a brittle behavior with unstable propagation is expected. $\delta_{50}/\delta_c >$ 1 means that the specimen will present a ductile behavior and a stable rupture is foreseen.

In Figure 10, the relation between the ratio δ_{50}/δ_c and the brittleness number s is shown for the experimental and numerical results presented in this work. In this plot, it clearly appears that for values of s higher than 1.5, ratios of δ_{50}/δ_c higher than 1.4 are obtained, therefore, indicating an evident ductile behavior for the specimen.

When s presents values between 0.7 and 1.5, the ratio δ_{50}/δ_c varies between 1.4 and 1; in these cases the specimens present a transitional ductile-to- brittle behavior.

Finally, when s is lower than 0.7, the ratio δ_{50}/δ_c will present values lower than 1.0, thus, characterizing a clear brittle behavior. It was noticed that, in this region, for several cases, the ratio δ_{50}/δ_c appears to be equal to 1.0. This is the typical value when the simulation is performed in a controlled displacement, when the specimen breaks in an unstable way and the snap-back branch of the curve is not captured. It is evident in the results of the Felser sandstone sets that, for specimens with s <1.0, a special displacement control allows to capture the snap-back branch during the softening.
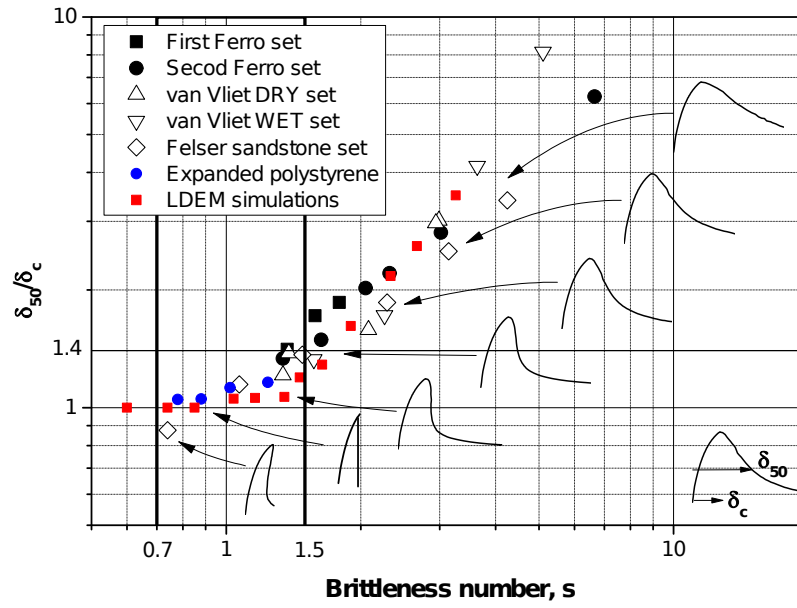
23

1

Figure 10: Relation between the Carpinteri brittleness number, *s*, and the shape of the global stress - displacement curve.

Finally, the ratio between the Carpinteri's number *s* computed for the specimen and the s_{LDEM} parameter computed in the context of the method is presented hereafter. In Figure 10, the ratio s/s_{LDEM} was plotted against the ratio d_{eq}/L, the latter measuring the relationship between the material length d_{eq}, that is a characteristic length of the material, as defined in section 2, and the size of the element that define the level of discretization used in the model.

In Figure 11, it is possible to verify in which way the variability of the fracture energy CV (G_f) influences the brittleness number *s* computed using the LDEM formulation. The simulations presented in section 4.1 were carried out using CV (G_f)=40%, this value is usually employed to simulate quasi-brittle materials such as concrete and rocks (see e.g. [36], [38]). Moreover, a particular study about the influence of the variability CV (G_f) was conducted in [30].

The white circle in Figure 11, illustrates the LDEM simulations presented in the present paper. A set of simulations presented in Ref. [50] were also added in red, together with other results presented in Refs. [68, 69] represented by gray circles.

Figure 11: Relation established between the global brittleness number and the brittleness number computed in the context of LDEM versus the ratio between the equivalent d value over the element size used in the discretization.

In Figure 11, it can be noticed that an approximate relationship between s/s_{LDEM} could be considered independent of d_{eq}/L, if $d_{eq}/L > 100$ ($\varepsilon_r/\varepsilon_p \approx 60$). For lower values of this ratio, the level of the discretization influences the s/s_{LDEM} result, finding responses in the interval [0.6, 1.5]. It is also important to notice that the influence of the fracture energy variation coefficient is significant.

When an element breaks, it generates a crack with a size related to its length, L. If this crack is smaller than the material equivalent length d_{eq}, it will not propagate until it reaches this critical dimension (after nucleation). If this crack size is closed to the material equivalent length d_{eq}, then it will propagate.

A s/s_{LDEM} greater than 1 indicates that the mean axial stress of all the LDEM elements (σ_p^*) is greater than the simulation maximum global stress (σ_p). This can be found with a more "brittle" constitutive model (ε_r close to ε_p or d_{eq} close to L) and/or large dispersions in a random field. With a large dispersion, it is easier to find a less resistant element than the mean element resistance. When the element breaks, if the generated crack is of the size of d_{eq}, a brittle fracture occurs. In this case, the simulation's

25

global response is close to the resistance of this first broken element, but much smaller than the mean resistance of all the other elements together.

Conversely, a s/s_{LDEM} smaller than 1 indicates that the mean axial stress of all the LDEM elements (σ_p^*) is less than the simulation maximum global stress (σ_p). This occur when we have little dispersion of the random field (low CV) and/or a "ductile" constitutive model (ε_r much larger than ε_p or d_{eq} bigger than L).

A practical application of the graphs presented in Fig 10 to calibrate the LDEM model could be proposed:

1- If experimental data about the material are available, together with the specimen size characterized by its R, the material properties G_f, E and the stress versus displacement global curve, then the value of s can be computed using the Eq. (1).

2- Assuming that $s_{LDEM} = s$ using the Eq. (14), it is possible to obtain the material parameter d_{eq}.

3- Adopting a level of discretization and the CV(G_f) to be used in the simulation, it is possible to compute d_{eq}/L and to obtain the ratio s/s_{LDEM} using the plot presented in Fig.11.

4- With the corrected value of s_{LDEM} and using Eq. (14), a better approximation of d_{eq} could be computed.

Notice that d_{eq} is a material parameter, and for this reason, if the model calibration is performed for one specimen, this value will not vary if the geometry and boundary conditions change.

In the present paper, a comparison between the global specimen behavior during damage process and the brittleness number is established. In [42, 50, 70] the link of the brittleness number with the dissipated energy and the final configurations obtained with LDEM simulations was also studied.

5. Conclusions

In the present work, several sets of experimental and numerical results are reviewed with the aim to correlate the Carpinteri's brittleness number obtained to predict the global behavior (ductile, brittle, or ductile-to-brittle transitional behavior).

In all cases, the specimens were subjected to pure tensile stress and heterogeneous materials were also analyzed. Experimental results produced by other researchers or by the authors themselves are presented. No pre-cracked specimens were considered, that is,

the spontaneous localization of the main crack was expected. The numerical approach used was a version of the Lattice Discrete Element Method that accounts for the random nature of the material employed. With this research work, it is possible to conclude that:

- A correlation between the s number and the aspect of the global force/stress versus displacement/strain curve is evident in all the evaluated cases. For this reason, the computation of s allows to predict what kind of behavior is to be expected for each specimen.

- The values computed using experimental and numerical results allow to perceive that for the boundary conditions used, when $s < 0.7$ is used as a lower bound, a global brittle behavior is expected. On the other hand, if $s > 1.5$, a ductile behavior is expected, moreover, in the interval of s [0.7, 1.5], a ductile-to-brittle transitional behavior occurs. The extension of the present study to verify the influence of the boundary condition and the specimen geometry will be the focus of future works.

- The relationship between the traditional definition of s and the definition of the brittleness number computed in the context of the numerical method used, s_{LDEM}, was presented. This relationship can be used to calibrate, in a consistent way, the LDEM method employed. It is possible to extend this methodology of calibration to other versions of the discrete element method (for example in Perydinamics), where spontaneous fracture can be also simulated.

- The satisfactory correlation between experimental and LDEM results confirms the robustness of this method as a numerical tool to model fracture processes in quasi-brittle materials.

Acknowledgments

REFERENCES

[1] Dugdale DS. Yielding of steel sheets containing slits. J Mech Phys Solids. 1960, 8:2, 100-104. https://doi.org/10.1016/0022-5096(60)90013-2.

[2] Boyle RW, Sullivan AM, Krafft JM. Determination of plane strain fracture toughness with sharply notched sheets. Welding J Res Suppl. 1962, 41, 428-432.

[3] Brown Jr WF, Srawley JE. Plane strain crack toughness testing of high strength metallic materials. ASTM Special Technical publication, No. 410, ASTM, Philadelphia, Pa. 1966.

[4] Mpalaskas AC, Matikas TE, Van Hemelrijck D, Papakitsos GS, Aggelis DG. Acoustic emission monitoring of granite under bending and shear loading. Archives of Civil and Mechanical Engineering. 2016, 16: 3, 313-324. https://doi.org/10.1016/j.acme.2016.01.006

[5] Mpalaskas AC, Thanasia OV, Matikas TE, Aggelis DG. Mechanical and fracture behavior of cement-based materials characterized by combined elastic wave approaches. Construction and Building Materials. 2014, 50, 649-656. https://doi.org/10.1016/j.conbuildmat.2013.10.022

[6] Carpinteri A. Static and energetic fracture parameters for rocks and concretes. Mat Constr. 1981, 14:81, 151-162. https://doi.org/10.1007/BF02473919.

[7] Carpinteri A. Application of fracture mechanics to concrete structures. Journal of the Structural Division (ASCE). 1982, 108: 4, 833-848.

[8] Carpinteri A. Post-peak and post-bifurcation analysis of cohesive crack propagation. Eng Fract Mech. 1989, 32: 2, 265-278. https://doi.org/10.1016/0013-7944(89)90299-3

[9] Carpinteri A. Cusp catastrophe interpretation of fracture instability. Journal of the Mechanics and Physics of Solids. 1989, 37: 5, 567-582. https://doi.org/10.1016/0022-5096(89)90029-X.

[10] Carpinteri A, Marenga C, Savadori A. Ductile-brittle transition by varying structural size. Eng Fract Mech. 1985, 21, 263-271. https://doi.org/10.1016/0013-7944(85)90015-3

[11] Carpinteri A. Scaling laws and renormalization groups for strength and toughness of disordered materials. Int J Solids Struct, 1994, 31(3), 291-302. https://doi:10.1016/0020-7683(94)90107-4

[12] Carpinteri A, Marega C, Savadori A. Size effects and ductile-brittle transition of polypropylene. J Mater Sci. 1986, 21: 4173-4178. https://doi.org/10.1007/BF01106526.

[13] Carpinteri A, Cornetti P, Barpi F, Valente S. Cohesive crack model description of ductile to brittle size-scale transition: dimensional analysis vs. renormalization group theory. Eng Fract Mech, 2003, 70, 1809-1839. https://doi.org/10.1016/S0013-7944(03)00126-7

[14] Brincker R, Henriksen MS, Christensen FA, Heshe G. Size Effects on the Bending Behaviour of Reinforced Concrete Beams. European Structural Integrity Society. 1999, 24, 127-137. https://doi.org/10.1016/S1566-1369(99)80064-8

[15] Gao H. Application of fracture mechanics concepts to hierarchical biomechanics of bone and bone-like materials. Int J Fract. 2006, 138, 101-137. https://doi.org/10.1007/s10704-006-7156-4.

[16] Corrado M, Cadamuro E, Carpinteri A. Dimensional analysis approach to study snap back-to-softening-to-ductile transitions in lightly reinforced quasi-brittle materials. A. Int J Fract. 2011, 172:1, 53-63. https://doi.org/10.1007/s10704-011-9646-2.

[17] Krajcinovic D. Damage Mechanics. Elsevier, Amsterdam, 1986.

[18] Seleson P, Beneddine S, Prudhomme S. A force-based coupling scheme for peridynamics and classical elasticity. Comp Mat Sci. 2013, 66, 34-49. https://doi.org/10.1016/j.commatsci.2012.05.016.

[19] Silling SA. Reformulation of elasticity theory for discontinuities and long-range forces. J Mech Phys Solids. 2000, 48, 175-209. https://doi.org/10.1016/S0022-5096(99)00029-0.

[20] Schlangen E, van Mier JGM. Crack propagation in sandstone: Combined experimental and numerical approach. Rock Mech Rock Engng. 1995, 28, 93-110. https://doi.org/10.1007/BF01020063.

[2] Krajcinovic D, Vujosevic M. Strain localization-short to long correlation length transition. Int J Solids Struct. 1998, 35, 31-32. https://doi.org/10.1016/S0020-9683(97)00307-7

[22] Sagar RV, Raghu Prasad BK. Modeling heterogeneity of concrete using 2D lattice network for concrete fracture and comparison with AE study. Sadhana. 2009, 34, 865-886. https://doi.org/10.1007/s12046-009-0052-7.

[23] Nagy E, Landis EN, Davids WG. Acoustic emission measurements and lattice simulations of microfracture events in spruce. Holzforschung, 2010, 64, 455-461. https://doi.org/10.1515/hf.2010.088.

[24] Rinaldi A. Advances in Statistical Damage Mechanics (SDM): New Modeling Strategies. In: Damage Mechanics and Micromechanics of Localized Fracture Phenomena in Inelastic Solids. CISM Courses and Lectures, vol 525. Springer, Vienna, 2011.

[25] Mastilovic S, Rinaldi A. Two-Dimensional Discrete Damage Models: Discrete Element Methods, Particle Models, and Fractal Theories. In: Voyiadjis G. (eds) Handbook of Damage Mechanics. Springer, New York, NY, 2015, 273-303.

[26] Riera JD. Local effects in impact problems on concrete structures. Proceedings of the Conference on Structural Analysis and Design of Nuclear Power Plants vol 3, Porto Alegre, October 3-5, 1984.

[27] Riera JD, Iturrioz I. Discrete element dynamic response of elastoplastic shells subjected to impulsive loading. Commun Numer Meth En. 1995, 11, 417-426. https://doi.org/10.1002/cnm.1640110506.

[28] Riera JD, Iturrioz I. Discrete element model for evaluating impact and impulsive response of reinforced concrete plates and shells subjected to impulsive loading. Nucl Eng Des. 1998, 179, 135-144. https://doi.org/10.1016/S0029-5493(97)00270-7.

[29] Kosteski LE, Riera JD, Iturrioz I, Singh RK, Kant T. Analysis of reinforced concrete plates subjected to impact employing the truss-like discrete element method. Fatigue Fract Eng M. 2015, 38, 276-289. https://doi.org/10.1111/ffe.12227.

[30] Kosteski LE, Iturrioz I, Cisilino AP, Barrios D'ambra R, Pettarin V, Fasce L, Frontini P. A lattice discrete element method to model the falling-weight impact test of PMMA specimens. Int J Impact Eng. 2016, 87, 120-131. https://doi.org/10.1016/j.ijimpeng.2015.06.011

[31] Schnaid F, Spinelli L, Iturrioz I, Rocha M. Fracture mechanics in ground improvement design. Ground Improvement. 2004, 8, 7-15. https://doi.org/10.1680/grim.2004.8.1.7

[32] Dalguer LA, Irikura K, Riera JD, Chiu HC. The importance of the dynamic source effects on strong ground motion during the 1999 Chi-Chi, Taiwan, Earthquake: Brief Interpretation of the Damage Distribution on Buildings. Bull Seismol Soc Am. 2001, 91: 5, 1112-1127. https://doi.org/10.1785/0120000705

[33] Dalguer LA, Irikura K, Riera JD. Simulation of tensile crack generation by three-dimensional dynamic shear rupture propagation during an earthquake. J Geophys Res. 2003, 108, No. B3, 2144. https://doi.org/10.1029/2001JB001738

[34] Iturrioz I, Birck G, Riera JD. Numerical DEM simulation of the evolution of damage and AE preceding failure of structural components. Eng Fract Mech. 2019, 210, 247-256 doi.org/10.1016/j.engfracmech.2018.02.023.

[35] Birck G, Riera JD, Iturrioz I. Numerical DEM simulation of AE in plate fracture and analogy with the frequency of seismic events in SCRs. Eng Fail Anal. 2018, 93, 214-223. https://doi.org/10.1016/j.engfailanal.2018.06.024

[36] Rios RD, Riera JD. Size effects in the analysis of reinforced concrete structures. Eng Struc. 2004, 26, 1115-1125. https://doi.org/10.1016/j.engstruct.2004.03.012

[37] Iturrioz I, Morquio A, Bittencourt E, Rosito d´Avila V. Performance of the Discrete Element Method to represent the scale effect. Published in Mechanics of Solids in Brazil 2007, Brazilian Society of Mechanical Sciences and Engineering. ISBN 978-85-85769-30-7, 2007, 247- 263.

[38] Iturrioz I, Miguel LFF, Riera JD. Dynamic fracture analysis of concrete or rock plates by means of the Discrete Element Method. Lat Am J Solids Stru. 2009, 6, 229-245.

[39] Iturrioz I, Riera JD, Miguel LFF, Kosteski LE. Scale Effects in Quasi-Fragile Materials Subjected to Compress. IASMiRT, SMiRT 21 - New Delhi, India. November 6-11, 2011

[40] Miguel LFF, Riera JD, Iturrioz I. Influence of size on the constitutive equations of concrete or rock dowels. Int J Numer Anal Meth Geomech. 2008, 32, 1857-1881. https://doi.org/10.1002/nag.699.

[41] Miguel LFF, Iturrioz I, Riera JD. Size effects and mesh independence in dynamic fracture analysis of brittle materials. CMES, 2010, 56, 1-16. 10.3970/cmes.2010.056.001

[42] Colpo AB, Kosteski LE, Iturrioz I. The size effect in quasi-brittle materials: Experimental and numerical analysis. Int J Dam Mech. 2017, 26, 395-416. https://doi.org/10.1177/1056789516671776.

[43] Kosteski LE, Barrios D'Ambra R, Iturrioz I. Determinación de parámetros fractomecánicos estáticos y dinámicos utilizando el método de los elementos discretos compuestos por barras. Rev int métodos numér cálc diseño ing. 2008, 24: 4, 323-343. URL https://www.scipedia.com/public/Kosteski_et_al__2008a.

[44] Kosteski LE, Barrios D'Ambra R, Iturrioz I. Fractomechanics parameter calculus using the Discrete Element Method. Lat Am J Solids Stru. 2010, 6, 301-321.

[45] Kosteski LE, Iturrioz I, Batista RG, Cisilino AP. The truss-like discrete element method in fracture and damage mechanics. Eng Computations. 2011, 28, 765-787. https://doi.org/10.1108/02644401111154664.

[46] Kosteski LE, Barrios D'Ambra R, Iturrioz I. Crack propagation in elastic solids using the truss-like discrete element method. I Int J Fract. 2012, 174, 139-161. https://doi.org/10.1007/s10704-012-9684-4.

[47] Riera JD, Miguel LFF, Iturrioz I. Strength of Brittle Materials under high strain rates in DEM simulations. CMES, 2011, 82, 113-136. 10.3970/cmes.2011.082.113

[48] Iturrioz I, Lacidogna G, Carpinteri A. Experimental analysis and truss-like discrete element model simulation of concrete specimens under uniaxial compression. Eng Fract Mech. 2013, 110, 81-98. https://doi.org/10.1016/j.engfracmech.2013.07.011

[49] Iturrioz I, Lacidogna G, Carpinteri A. Acoustic emission detection in concrete specimens: Experimental analysis and lattice model simulations. Int J Dam Mech. 2014, 23, 327-358. https://doi.org/10.1177/1056789513494232

[50] Birck G, Iturrioz I, Lacidogna G, Carpinteri A. Damage process in heterogeneous materials analyzed by a lattice model simulation. Eng Fail Anal. 2016, 70, 157-176. https://doi.org/10.1016/j.engfailanal.2016.08.004

[51] Da Silva GS, Kosteski LE, Iturrioz I. Analysis of the failure process by using the Lattice Discrete Element Method in the Abaqus environment. Theoretical and Applied Fracture Mechanics. 2020, 107, 102563. https://doi.org/10.1016/j.tafmec.2020.102563

[52] Nayfeh AH, Hefzy MS. Continuum modeling of three-dimensional truss-like space structures. AIAA Journal. 1978, 16, 779-787. https://doi.org/10.2514/3.7581

[53] Rinaldi A, Krajcinovic D, Peralta P, Lai YC. Lattice models of polycrystalline microstructures: a quantitative approach. Mech Mater. 2008, 40, 17-36. https://doi.org/10.1016/j.mechmat.2007.02.005.

[54] Rocha MM, Riera JD, Krutzik NJ. Extension of a model that aptly describes fracture of plain concrete to the impact analysis of reinforced concrete. Int. Conf. and Structural Mechanics in Reactor Technology, SMiRT 11, Trans. Vol. J., Tokyo, Japan. 1991.

[55] Hillerborg A. A model for fracture analysis. Cod LUTVDG/TV BM-3005, 1-8. 1978.

[56] Kupfer HB, Gerstle KH. Behavior of concrete under biaxial stresses. J Eng Mech Div. 1973, 99: 4, 853-866.

[57] Kanninen MF, Popelar CH. Advanced Fracture Mechanics. Oxford University Press. 1985. ISBN 0-19-503532-1.

[58] Silling SA, Epton M, Weckner O, Xu J, Askari E. Peridynamic States and Constitutive Modeling. J Elasticity, 2007, 88, 151-184. https://doi.org/10.1007/s10659-007-9125-1

[59] Taylor D. The Theory of Critical Distances: A New Perspective in Fracture Mechanics, Elsevier. 2007.

[60] Puglia VB, Kosteski LE, Riera JD, Iturrioz I. Random field generation of the material properties in the lattice discrete element method. J Strain Anal Eng, 2019, 54: 4, 236-246 https://doi.org/10.1177/0309324719858849

[61] Iturrioz I, Riera JD, Miguel LFF. Introduction of imperfections in the cubic mesh of the truss-like discrete element method. Fatigue Fract Eng M. 2014, 37: 5, 539-552. https://doi.org/10.1111/ffe.12135

[62] Carpinteri A, Ferro G. Size effects on tensile fracture properties: A unified explanation based on disorder and fractality of concrete microstructure. Mater Struct. 1994, 27, 563-571. https://doi.org/10.1007/BF02473124

[63] Carpinteri A, Ferro G. Scaling behaviour and dual renormalization of experimental tensile softening responses, Mat. Struct. 1998, 31, 303-309. https://doi.org/10.1007/BF02480671

[64] van Vliet MRA. Size effect in tensile fracture of concrete and rock. Ph.D. Thesis, Delft University of Technology, Delft, The Netherlands. 2000.

[65] van Vliet MRA, van Mier JGM. Size effects of concrete and sandstone. Heron, 2000, 45, 91-108. http://resolver.tudelft.nl/uuid:f2beb295-f41d-4db1-b126-8be73c23317b

[66] Carpinteri A, Maradei F. Three-jack solution to obtain a truly stable and symmetric tensile concrete test. Experimental Mechanics. 1995, 35, 19-23. https://doi.org/10.1007/BF02325829

[67] Birck G, Iturrioz I, Riera JD, Miguel LFF. Influence of mesh orientation in discrete element method simulations of fracture processes. J Strain Anal Eng Des. 2018, 53: 6, 400-407. https://doi.org/10.1177/0309324718775284

[68] Kosteski LE. Aplicação do Método dos Elementos Discretos formado por barras no estudo do colapso de estruturas. Doctoral Thesis, Universidade Federal de Rio Grande do Sul, Porto Alegre, 2012 (in Portuguese). http://hdl.handle.net/10183/56589

[69] Maders L, Kosteski LE, Iturrioz I. Estudo do efeito de escala no método dos elementos discretos formado por barras. In: Mecom 2012, Salta, Argentina. Mecánica Computacional v. XXXI, 1857-1876.

[70] Birck G, Rinaldi A, Iturrioz I. The fracture process in quasi-brittle materials simulated using a lattice dynamical model. Fatigue Fract Eng Mater Struct. 2019, 42: 12, 2709-2724. https://doi.org/10.1111/ffe.13094

Declaration of interests

☒ The authors declare that they have no known competing financial interests or personal relationships that could have appeared to influence the work reported in this paper.

☐The authors declare the following financial interests/personal relationships which may be considered as potential competing interests:

Size Effect in Heterogeneous Materials analyzed through a Lattice Discrete Element Method Approach

Luis Eduardo Kosteski[a], Ignacio Iturrioz[b], Giuseppe Lacidogna[c], Alberto Carpinteri[d]

[a] Associate Prof., Eng., Dr., PPEng, UNIPAMPA, Alegrete, RS, Brazil, luiskosteski@unipampa.edu.br.
[b] Full Prof., Eng., Dr., PROMEC, UFRGS, Porto Alegre, RS, Brazil, ignacio@mecanica.ufrgs.br
[c] Associate Prof., Arch., Dr., Department of Structural, Geotechnical and Building Engineering, Politecnico di Torino, Turin, Italy, giuseppe.lacidogna@polito.it
[d] Full Prof. Department of Structural, Geotechnical and Building Engineering, Politecnico di Torino, Turin, Italy, alberto.carpinteri@polito.it

Corresponding author´s e-mail: luiskosteski@unipampa.edu.br

Abstract

In the Lattice Discrete Element Method (LDEM), different types of mass are considered to be lumped at nodal points and linked by means of one-dimensional elements with arbitrary constitutive relations. In previous studies on the tensile fracture behavior of rock samples, it was verified that numerical predictions of fracture of non-homogeneous materials using LDEM models are feasible and yield results that are consistent with the experimental evidence available so far. In the present paper, a discussion of the results obtained with the LDEM is presented. A set of rock specimens of different sizes, subjected to monotonically increasing simple tensions, are simulated with LDEM. The results were analyzed from the perspective of the brittleness number, proposed by Alberto Carpinteri, to measure the brittleness level of the structure under study. The satisfactory correlation between the experimental results and LDEM results confirms the robustness of this method as a numerical tool to model fracture processes in quasi-brittle materials.

Keywords: Heterogeneous Materials, Lattice Discrete Element Method, Size Effect , Brittleness Number.

Nomenclature

A_i — Cross-section area of the element to obtain the mechanical equivalence with the solid (*i=l*, longitudinal bars; *i=d*, diagonal bars).

A_i^* — Cross section to obtain the fracture equivalence with the solid material.

b, D, d, r — Dimensions that define the specimens' geometries.

d_{eq} — Characteristic length of the material.

1   E, ν Elastic constant: Young's modulus and Poisson's ratio, respectively.

2   ECL Elemental Constitutive Law.

3   F Element axial force.

4    $F(t), P(t)$ Internal and external vector forces.

5   F_{max} The peak force measured in each bar.

6   G_f Fracture Energy

7   K_c The critical stress intensity factor.

8   L Length of the side of the cubic LDEM module.

9   L_{corr} The correlation length.

10   L_d Length of the diagonal elements.

11   LDEM   Lattice Discrete Element Method.

12   M, C Mass and damping matrices.

13   q The critical crack size.

14   R Structure characteristic length.

15   s, s_E Both version of the brittleness numbers proposed by Carpinteri

16   s_{LDEM} Brittleness number computed in the context of LDEM.

17   w Displacement.

18   $\ddot{x}, \dot{x}$ Nodal acceleration and velocity vectors.

19   Y The shape coefficient.

20   Z Specimen length or span.

21   Z/R The slender coefficient of the specimen.

22   $\delta_c, \delta_{50}, \delta_u$ Characteristic displacements measured in the LDEM global stress-

23   displacement responses.

24   ε_p Characteristic strain measured in each bar.

25   ε_r Failure strain measured in each bar.

26   ε_u Strain linked with σ_p.

27   ρ Specific mass.

28   σ Stress.

29   σ_p Global maximum strength

30   σ_p^* The stress that correspond with the ε_p

31   $\mu(.), CV(.)$ Mean value and variation coefficient.

32

1. Introduction

In the literature, the scale effects were extensively studied to connect the fracture process zone with the specimen size, the pioneer works of Dugdale [1], Boyle [2], and Brown and Srawley [3] could be cited among others. More specifically, in the so-called quasi-brittle materials, such as concrete, this topic was also widely discussed. This kind of materials are characterized by a disordered microstructure, exhibits damage localization, and are unable to present plastic or hardening deformations, having a non-negligible fracture process zone compared to the structure size. Furthermore, it was observed that the structural behavior changes with the size of the analyzed specimen. Also the link between acoustic emission parameters and the ultimate strength was shown experimentally, among others by Mpalaskas [4, 5], and this relation could be proposed for better understand the damage process in quasi-brittle materials.

Carpinteri [6-10] proposed dimensionless parameters: the brittleness numbers s and s_E, to measure the structural brittleness that describes the susceptibility of cracks to propagate in unstable conditions. These numbers are related to the change of behavior with the structural size and depend on the fracture energy and the yielding strength of the material as well as on the characteristic dimension of the structure:

$$s_E = \frac{G_f}{\sigma_p R}; \qquad s = \frac{K_c}{\sigma_p R^{1/2}}. \tag{1}$$

In these expressions, K_c is a measure of toughness, and G_f is a mechanical characteristic of brittle materials called fracture energy, following the nomenclature used by Carpinteri in his Cohesive Crack Model presented in [9, 11], σ_p represent the yielding or maximum stress, and R constitutes the characteristic structural dimension that defines the specimen's size. If we consider that $K_c = (G_f E)^{0.5}$ and $\sigma_p = E\varepsilon_u$, then the equivalence between the two adimensional numbers is:

$$s_E = s^2 \varepsilon_u, \tag{2}$$

where ε_u is the strain linked to σ_p.

Both nondimensional numbers have been used in several scientific papers in the last three decades [12-16, among others]. In Carpinteri [6, 7], the characteristics of these parameters are presented in detail, and the recommendation that s_E is more adequate to be used for brittle or quasi-brittle materials and s for ductile materials is highlighted. In the present work, the s instead of s_E parameter was used to measure the change of global behavior in the specimens that were tested and consequently simulated by the model.

1   The numerical simulations of structures made of quasi-brittle materials have the

2   implication that, in these materials, the characterization of the damage is often governed

3   by more than one single crack. The studies of a set of small fractures interacting at

4   different scale levels have great relevance when attempting to understand and simulate

5   the behavior of these materials. As mentioned by Krajcinovic [17], accounting for each

6   individual crack in the heterogeneous materials, assessing its influence on the structural

7   response and ultimately on the structural failure, is not a task that can be approached by

8   using conventional methods of analysis in solid mechanics. In this way, the methods,

9   which are able to represent naturally the discontinuities, could be an alternative method

10   of analysis. Among the non-conventional methods of continuous representation,

11   Peridynamics is widely used. Such method belongs to the family of Discrete Element

12   Methods. In this approach, the combination of nodes and associated discrete mass by

13   means of an interaction law applied between neighbor nodes represents the continuum.

14   The proposal carried out for the Peridynamics was used originally to represent the

15   interaction force at the atomic level. Seleson [18] could be cited here as an example of

16   this approach. Moreover, the same approach was also applied at large scale levels, all

17   thanks to the pioneering work by Silling [19].

18   Another equivalent discrete approach is the Truss-like Discrete Element Method

19   or Lattice Model. Various and relevant approaches study can be referred to; among others

20   like the ones proposed by Schlangen and van Mier [20], Krajcinovic and Vujosevic [21],

21   and, more recently, the works of Sagar and Prasad [22], Nagy *et al.* [23], and Rinaldi [24].

22   A review of the different versions of Discrete Element Method, including the Particle

23   methods and Lattice approaches, is presented in Mastilovic and Rinaldi [25].

24   In the present paper, a version of the Lattice Discrete Element Method (LDEM)

25   proposed by Riera [26] will be used. This method was developed originally to determine

26   the dynamic response of plates and shells when failure occurs primarily by shear or

27   tension under a shock wave caused by impact loading, as it is generally observed in

28   concrete structures.

29   In the LDEM, the quantities of mass are considered lumped at nodal points and

30   linked by means of one-dimensional elements with arbitrary constitutive relations. The

31   satisfactory correlation between the experimental results and the LDEM predictions

32   confirms the robustness of this method as a numerical tool to model fracture processes in

33   quasi-brittle materials. These findings were reported, among others, in a successful

34   analysis of: shells subjected to impulsive loading [27-30], the fracture of elastic

foundations on soft sand beds [31], the generation and propagation of an earthquake [32-35], the study of the scale effect in quasi-brittle materials [36-42]; the computation of fracture parameters in static and dynamic problems [43-46], the study of strength of brittle materials under high strain rates [47] and finally the acoustic emission events in quasi-brittle materials [34, 35, 48-50]. In Refs. [29-31, 36, 46, 51], LDEM simulations were discussed in which quantitative comparison with experimental results in terms of global parameters, such as displacement versus loads or final configurations, are presented. The following section presents a brief description of the theoretical foundation of this method.

2. Lattice Discrete Element Method Formulation

The Lattice Discrete Element Method (LDEM), used in the present work, represents the continuum by means of a 3D lattice, that is, a periodic spatial arrangement of bars with amounts of mass lumped at their ends. Figure 1 shows the discretization strategy in which the stiffness of the LDEM elements, corresponding to an equivalent orthotropic linear elastic material, was obtained by Nayfeh and Hefzy [52]. The basic cubic module is built with twenty bars and nine nodes. Each node presents three degrees of freedom given by the spatial components of the displacement vector in the global reference system.

(a)   *(b)*
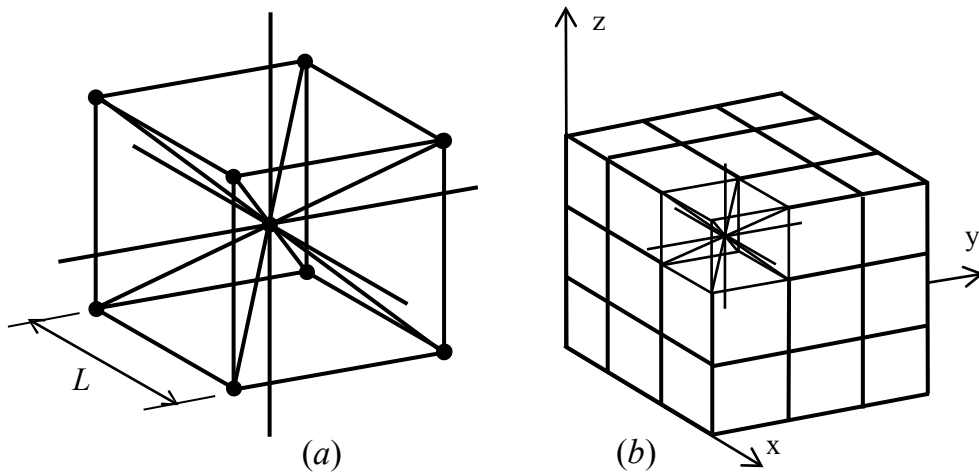
Figure 1- LDEM discretization strategy: (a) basic cubic module, (b) generation of the prismatic body.

In case of an isotropic elastic material, the cross-sectional area A_l of the longitudinal elements (those defining the edges of the module and those that are parallel to the edges connected to the node located at the center of the module) in the equivalent discrete model is:

$$A_l = \phi L^2, \tag{3}$$

where L is the length of the side of the cubic module under consideration. The function $\phi = (9 + 8\delta)/(18 + 24\delta)$, where $\delta = 9\nu/(4 - 8\nu)$ accounts for the effect of the Poisson's ratio ν [49, 30]. Similarly, the area A_d of the diagonal elements is:

$$A_d = \phi L_d^2 = \frac{2}{\sqrt{3}}\delta\phi L^2, \tag{4}$$

were $L_d = \frac{2}{\sqrt{3}}L$ is the length of the diagonal elements. The coefficient $2/\sqrt{3}$ in Eq. (4) accounts for the difference in length between the longitudinal and the diagonal elements.

It is important to point out that, for $\nu = 0.25$, the correspondence between the equivalent discrete solid and the isotropic continuum is complete. On the other hand, for values of $\nu \neq 0.25$ discrepancies appear in the shear terms. These discrepancies are small and may be neglected in the range $0.20 \leq \nu \leq 0.30$. For values of ν outside this range, a different basic module should be used (see Ref. [52]). It is interesting to note that while no lattice model can exactly represent a locally isotropic continuum, it can also be argued that no perfect locally isotropic continuum exists in the physical world. Isotropy in solids is a bulk property that reflects the random distribution of the orientation of constituent elements. A comprehensive study on the effect of the LDEM lattice geometry on the value of the Poisson's ratio can be found in Ref. [53].

The equations of motion are obtained from equilibrium conditions of all forces acting on the nodal mass, resulting in a system of equations of the form:

$$M\ddot{x} + C\dot{x} + F(t) - P(t) = 0, \tag{5}$$

where $\ddot{x}$ and $\dot{x}$ are, respectively, the nodal acceleration and velocity vectors; M and C are the mass and damping matrices, respectively, and the vectors $F(t)$ and $P(t)$ convey the nodal internal and external forces. Since M and C are diagonal, the equations in Eq. (5) are not coupled, and they can be easily integrated in the time domain using an explicit finite difference scheme.

It is worth noting that, since the nodal coordinates are updated at each time step, large displacements are accounted for naturally. The convergence of LDEM solutions in linear elasticity and elastic instability problems was verified by [32], among others.

The irreversible effects of crack nucleation and propagation that occur in brittle or quasi-brittle materials were taken into account by [54], and more recently by [45], through the introduction of a non-linear constitutive model that reduces the element load

carrying capacity. More details of this implementation can be found in [43-46, 54], among others.

Based on Hillerborg's theory [55], the bilinear model for quasi-brittle materials used in this work is shown in Figure 2. In case of tensile loads, the area under the force - strain curve (the area of the OAB triangle in Figure 2) is the energy density necessary to fracture the area of element influence, the fracture energy. Thus, for a given point P on the force - strain curve, the area of the OPC triangle represents the reversible elastic energy density stored in the element, while the area of the OAP triangle is the dissipated fracture energy density. One element fails and loses its load carrying capacity when the dissipated energy density equals the fracture energy.
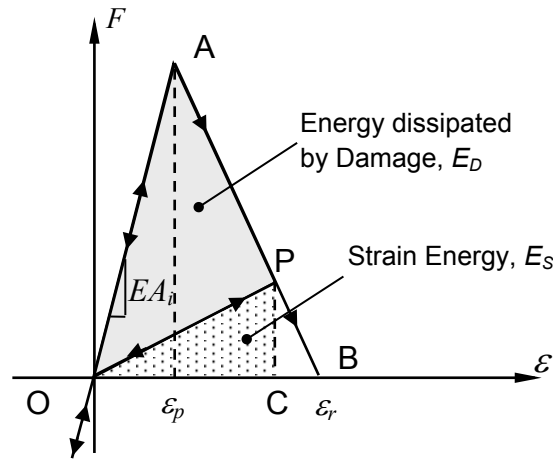
Figure 2: Bilinear constitutive model with material damage.

In the case of compressive loads, the material behaves in a linear elastic manner. In this way, the failure in the compression is induced by indirect traction. In quasi-brittle materials, this assumption is reasonable because its ultimate strength in compression is usually five to ten times larger than that in tension [56].

In the constitutive model presented in Figure 2, F is the element axial force, and A_i the cross-section area of the element, depending whether longitudinal or diagonal element is considered, as in Eq. (3) and Eq. (4). In this model, the fracture energy per unit area coincides with the material fracture energy, G_f.

The so called critical strain ε_p, as illustrated in Figure 2, is the maximum strain before damage initiation. The critical strain is a micro-parameter, that is, a parameter that governs the constitutive law at the elemental level. The *limit strain* ε_r is the strain value for which the elements lose its load carrying capacity (point B in Figure 2). The limit strain is much greater than or equal to the critical strain. This value is calculated to satisfy

the fact that the dissipated energy density released when the element fail must be equal to the multiplication of the equivalent fracture area of the element, A_i^*, times the fracture energy, G_f, divided by the element length, L, that is:

$$\int_0^{\varepsilon_r} F(\varepsilon)d\varepsilon = \frac{G_f A_i^*}{L_i}. \tag{6}$$

The index i in the expression indicates it either refers to longitudinal or the diagonal elements.

The area below the bilinear model is $\varepsilon_r \varepsilon_p E A_i / 2$, then, the final strain defined for the element ε_r, illustrated in the Figure 2, is designated as:

$$\varepsilon_r = \frac{G_f}{\varepsilon_p E}\left(\frac{A_i^*}{A_i}\right)\left(\frac{2}{L_i}\right), \tag{7}$$

A_i^* denotes the equivalent fracture area of each element defined in order to satisfy the condition that the energy dissipated by the fracture of the continuum and by its discrete representation are equal, $A_i^* = \frac{3}{22} L_i^2$. This deduction can be found in [45]. It should be noted that ε_r depends on the material properties and on the level of discretization.

Young's modulus E, the stress intensity factor K_c and the critical stress σ_p are related by the classical fracture mechanic expression [57] given below:

$$K_c = \sigma_p Y \sqrt{\pi q}, \tag{8}$$

in which Y is a parameter that accounts for the influence of the boundary conditions and the orientation of the critical crack size q. If it is assumed that the behavior up to the beginning of the rupture is linear, then $\sigma_p^* = E\varepsilon_p$ and, recalling the equivalence between K_c and the fracture energy G_f, we obtain the expression:

$$\sqrt{G_f E} = E\varepsilon_p Y \sqrt{\pi q}. \tag{9}$$

This assumption is very important for this development because the tension obtained ($\sigma_p^* = E\varepsilon_p$) is not the global maximum strength σ_p, as defined in Eq. (1), but instead, is a local or elemental maximum.

In order to simplify Eq. (9), an equivalent length d_{eq} is defined as follows:

$$d_{eq} = q\pi Y^2. \tag{10}$$

Substituting Eq. (9) in (10), then:

$$d_{eq} = \frac{G_f}{(\varepsilon_p)^2 E} \tag{11}$$

Eq. (11) indicates that d_{eq} may be regarded as a material property, since it does not depend on the discretization level, representing in fact a *characteristic length of the*

1   *material* (similar as the width of the plasticity region in the crack tip in the Dugdale

2   model).

3   It also is possible to isolate ε_p from the Eq. (11) to obtain:

4     $$\varepsilon_p = \sqrt{\frac{G_f}{d_{eq}E}},\qquad\qquad\qquad (12)$$

5   and replacing (11) in ε_r Eq. (7) it is found:

6     $$\varepsilon_r = \varepsilon_p d_{eq}\left(\frac{A_i^*}{A_i}\right)\left(\frac{2}{L_i}\right),\qquad\qquad (13)$$

7   Eq. (12) shows that maintaining E and G_f constant, when the d_{eq} increases, a more ductile

8   behavior is expected. The area below the elemental constitutive relation (see Fig. 2) is

9   linked to G_f, then, if this parameter remains constant, the decrease of ε_p has to be

10   compensated by increasing the value of ε_r to maintain the area below the curve.

11   When ε_p is equal to ε_r, the minimum area of bilinear constitutive model is

12   obtained, that is, the limit relation between the equivalent length and the element length,

13   for longitudinal elements, is found to be $d_{eq} \geq \frac{15}{22}L$. In some way, from the Eq. (13) it is

14   possible to say that $\varepsilon_r/\varepsilon_p \propto d_{eq}/L$, that is, d_{eq}/L is related to the bilinear constitutive

15   model. If the constitutive model is "brittle" (ε_r next to ε_p), d_{eq}/L will be small, however,

16   if the constitutive model is "ductile" (ε_r much larger than ε_p) d_{eq}/L will be higher.

17   It can be noticed that a characteristic length as material parameter is also discussed

18   in another version of the discrete element method called Peridynamics, proposed by

19   Silling *et al.* [58]. In this method, there is a set of nodes where the mass are discretized

20   and linked with bars, moreover, the level of neighboring among nodes is given by a

21   material parameter called horizon. This parameter depends on the discretization level

22   used to define the quantity of nodes linked to one and another. The horizon physical

23   meaning is analogous to the meaning of the d_{eq} in the version of the Discrete Element

24   Method used in the present work.

25   Taylor [59] considers that a breaking criterion is fulfilled when a dominium

26   portion, defined by a characteristic dimension, reaches the critical level of stress. In this

27   approach, both parameters are considered as material parameters. The link between the

28   characteristic distance of this author and the d_{eq} is evident.

29   The randomness of the model is introduced considering G_f as a random field with a

30   Weibull density function characterized by its mean value $\mu(G_f)$ and variation coefficient

1 $CV(G_f)$. Moreover, it is necessary to consider the spatial correlation function of this

2 random parameter. How to consider the random nature in the model could be explained

3 in [30, 60].

4   In the model here implemented, the random values of G_f assigned to every element

5 have statistical independence, that is, the random properties of one element do not depend

6 on the properties of the other neighboring elements. This assumption is equivalent to

7 consider that the correlation length is $L_{corr} = 0.3L$. Notice that when randomness is

8 introduced in G_f, indirectly randomness is also introduced in ε_p (see Eq. 12). In this way,

9 the maximum strength of an element $F_{max} = EA_i\varepsilon_p$, which is directly related to point A

10 in Figure 2, is also random. The axial stress of the element will be: $\sigma_p^* = E\varepsilon_p$. Another

11 alternative to introduce the random nature in the model is to consider geometric

12 perturbation in the mesh, about this aspect see [61]. More detail about the LDEM

13 formulation can be found in Ref. [50].

14   Below, several points are explained to clarify the meaning of the parameters used in

15 the definition for the constitutive law of the LDEM model:

16 (i) The concept of the brittleness number s in the context of LDEM is introduced with the

17   aim of showing evidence of the physical meaning of the parameter d_{eq} previously

18   defined.

19   If we rewrite the Eq. (1) that introduces the *brittleness number s* proposed by

20   Carpinteri [6], we consider that $\sigma_p = \sigma_p^*$ and recalling the equivalence between K_c

21   and the fracture energy G_f, the expression of s in the context of the LDEM

22   formulation will be:

23 $$s_{LDEM} = \frac{K_c}{\sigma_p^* R^{1/2}} = \frac{\sqrt{G_f E}}{E\varepsilon_p R^{1/2}} = \sqrt{\frac{d_{eq}}{R}}. \quad\quad (14)$$

24   From this expression it can be interpreted that, if a crack of a size $> d_{eq}$ appears

25   during the damage process in a structure with a characteristic dimension R, it will

26   propagate in an unstable form, suggesting a brittle global structural behavior.

27   However, this situation will only be possible if d_{eq} is lower than R. If this condition

28   is not fulfilled, it will not be possible to have a crack with a dimension similar to d_{eq},

29   because there is not enough space in the structure for crack propagation. In the latter

30   situation, the structure will have a ductile behavior during its damage process. The

31   structure boundary condition influences this relation but it does not change the

32   general tendency.

The ratio between Eq. (1) and (14) allows writing the relationship between the traditional expression of the brittleness s with its definition in the context of LDEM. As it was previously emphasized, the difference resides in the definition of σ_p: in the classical expression of s, σ_p is the stress value in which the material collapses, while in the s_{LDEM} definition, $\sigma_p = \sigma_p^*$ is the axial stress of the elements. The ratio s/s_{LDEM} is a function of the statistical and spatial distribution of the random field that characterizes G_f, and the shape of the elemental constitutive law used. At the end of the present work, a further comment about this ratio is provided.

(ii) In contrast to the usual practice used in the Finite Element Method, the constitutive relationship in the LDEM is not only a function of the material properties. The LDEM model considers the following macroscopic parameters: the elastic modulus E, the fracture energy G_f, and the characteristic length d_{eq}. With these three parameters using Eq. (12), the critical strain ε_p, where the bar force reaches its maximum value is computed (see Fig 2). Multiplying E by the Eq. (3) and (4) the linear pre-peak relation in the elemental constitutive law (ECL), defined by EA_i, is indicated in Figure 2. The fracture energy G_f directly influences in the area below the ECL, as it is indicated in Eq. (6). Furthermore, using Eq. (13) as illustrated in Fig. 2, the characteristic length of the material, d_{eq}, defines the post-peak branch in the ECL by means of the local parameter ε_r. Notice that not only ε_r, but also EA_i depend on the discretization level.

(iii) Another interesting feature of the method is that, although it uses a scalar damage law to describe the uniaxial behavior of the elements, involves a global model that takes into account of the anisotropic damage. This is because, when the uniaxial bars, oriented in different directions, are damaged they modify their axial stiffness, allowing to represent an anisotropic global behavior.
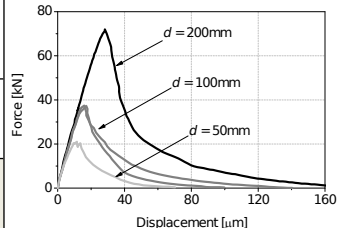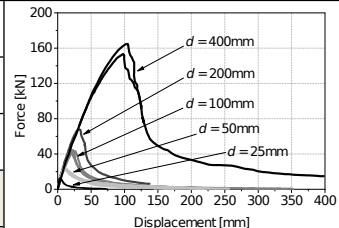
3. Experimental background

The results obtained by Carpinteri and Ferro [62, 63], van Vliet [64] as well as van Vliet and van Mier [65], all of whom have studied the scale effects on tensile strength of concrete and rock, are used to explore the link between the brittleness number, s, proposed by Carpinteri [6, 7] and the global behavior obtained in the cited cases that could be classified as ductile or brittle. Experimental results obtained by the authors over expanded polystyrene samples are also described and analyzed.

1 **3.1 Carpinteri and Ferro Results**

2   Carpinteri and Ferro [62, 63] and Carpinteri and Maradei [65] carried out two sets

3 of tests with specimens of several sizes. The Young's Modulus was measured from the

4 global stress versus strain curves, at around 35GPa for the two sets. The material

5 parameters and the brittleness number values s, computed using Eq. (1), are presented in

6 Table 1. The characteristic dimension R was considered in the present case as the

7 dimension of the specimen neck, d.

8   In both series, the specimen with characteristic size d smaller than 100 mm

9 showed a ductile behavior, whereas specimens with d larger than 200 mm showed a

10 quasi-brittle behavior. In both sets of results s <1.4 indicates a quasi-brittle global

11 behavior

12

13 Table 1: Material parameters, the brittleness number computed and the curves used as
14 sources of information for the experimental sets 1 and 2 presented by Carpinteri and
15 Ferro [62, 63]. (E=35 GPa).

d [mm]	σ_p [MPa]	G_f [N/m]	s	Experimental Results	Specimen Geometry
Set 1					
50	4.25	83	1.79		
100	3.78	102	1.58		
200	3.64	142	1.37		
Set 2					
25	4.79	147	2.99		
50	4.56	257	2.94		
100	4.37	236	2.08		
200	3.80	158	1.38		
400	3.72	286	1.34		

16

17

18 **3.2 van Vliet and van Mier's Results**

19   van Vliet [64] performed three sets of tests of specimens using different

20 dimensions, as is shown in Fig. 3. The first set was conducted by using concrete stored in

21 the laboratory in a dry environment, called the DRY set. The second set also was with

1 concrete, however stored in a climate room, called the WET series. Finally, the third set

2 of specimens consists of Felser sandstone specimens called FELSER.

3   For the calculus of the brittle number, the fracture energy G_f measured

4 extrapolating the stress opening curve (σ-w) was used. The material parameters and the s

5 values computed are presented in Table 2. In the present cases, the characteristic

6 dimension R to compute the brittleness number s with the Eq. (1) is $0.6D$, the specimen

7 neck, as could be appreciated in Fig 3.

8

9

Type	A	B	C	D	E	F
D [mm]	50	100	200	400	800	1600
r [mm]	36.25	72.5	145	290	580	1160

10 Figure 3. Specimen shape and dimensions for van Vliet [64] adopted size range.

11

12   For all the van Vliet experiments, represented in Table 2, it is possible to observe

13 an apparent change in the global behavior for specimen with brittle number s near to 1.5.

14 For s values lower than 1.6, specimen F ($s = 1.34$) for the DRY set, specimen D ($s = 1.57$)

15 for the Wet set and specimens D ($s = 1.48$), E ($s = 1.07$) and F ($s = 0.74$) for the FELSER

16 set, the global response seems to be brittle. Finally, for s values higher than 1.6, a clearly

17 ductile global response is observed.

18   In fact, it is possible to consider that with s between 2 to 1 we are in a transition

19 zone, and a very clear brittle behavior could be defined when s is lower than 1, as seen

20 for the F($s = 0.74$) specimen in the FELSER set.

21

Table 2: Material parameters and brittleness number computed for the van Vliet [64] specimens.

Type	σ_p [MPa]	G_f [N/m]	E [GPa]	s	
DRY set					
A	2.54	97.0	88.42	6.66	
B	2.97	125.7	38.5	3.02	
C	2,75	124.2	39.41	2.32	
D	2.30	125.2	42.80	2.05	
E	2.07	142.3	38.25	1.63	
F	1.86	141.1	42.55	1.34	
WET set					
A	2.17	91.1	40.48	5.11	
B	2.23	99.6	39.80	3.64	
C	2.48	88.9	42.38	2.26	
D	2.37	100.4	33.25	1.57	
FELSER sandstone set					
A	0.82	76.7	4.75	4.25	
B	1.22	111.3	7.90	3.14	
C	1.01	93.8	6.87	2.29	
D	0.96	135.1	3.60	1.48	
E	1.30	143.9	6.50	1.07	
F	1.20	93.2	8.23	0.74	

3.3 Expanded polystyrene experimental results

In the following section, a set of tests carried out by the authors on expanded polystyrene are presented. The material was submitted to direct tensile stress using specimens with the same geometry, but different sizes compared to the ones used by Van Vliet [64]. The tests were carried out in a Universal Machine Test Shimadzu AGS - X 5 kN in the Federal University of Pampa - Brazil.

In Table 3 the dimensions of the body tests called A, B, C and D are presented. Four tests were conducted for each configuration. For all the four specimen geometries, the thickness was always 9 mm. The specimens were fixed at the ends, as illustrated in

14

Table 3 by applying the prescribed displacement at the top end at a constant displacement rate of 0.0333 mm/min.

Table 3. Body test dimensions.
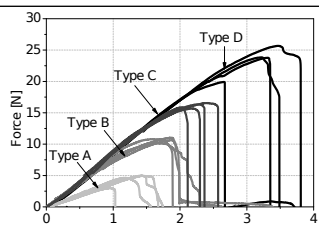
Type	A	B	C	D
D [mm]	10	20	30	45
r [mm]	7.25	14.5	21.75	32.63

Fracture energy G_f equal to 25N/m, value also adopted by Colpo *et al.* [42], was used for the calculus of the brittleness number by using Eq. (1). These results are presented in Table 4. As done in previous tests, the specimen characteristic length R was considered to be equal to the neck specimen, $0.6D$.

A similar tendency, to what was observed in previous cases, was also appreciated in the results obtained using expanded polystyrene. When the s value is lower than 1, the global stress curve clearly shows a brittle behavior, and when the results of s are between the interval 2.0 to 1.0, a transition behavior is observed.

Table 4: The brittleness number computed for the set of test carried out over expanded polystyrene specimens.

Type	σ_p [MPa]	CV [%]	E [N/mm²]	CV [%]	s	
A	0.049	21.4	0.89	12.1	1.24	
B	0.059	3.4	1.73	8.4	1.02	
C	0.060	2.5	2.01	12.8	0.88	
D	0.058	10.4	2.21	9.3	0.78	

With the aim of categorizing the global behaviors in all the tests carried out, a typical brittle global response it is considered when:

It is important to highlight here that, in Carpinteri [6, 7], the author reaches the conclusion that, for specimens subjected to tension or compression, the following equation

$$\frac{s_E}{\left(\frac{Z}{R}\right)\varepsilon_u} \leq \frac{1}{2}, \tag{15}$$

defines the condition for Snap-Back instability that governs the global mechanical behavior. In the Eq. (15), Z is the specimen length or span and Z/R represents the slenderness. For the cases studied in the present work, Z/R is always considered close to 1. Remembering the equivalence given between s_E and s presented in Eq. (2), Eq. (15) could be rewritten in terms of s as $s^2 \leq 1/2$, i.e. $s \leq 1/\sqrt{2} \sim 0.7$, a result that could be considered as a lower bound for the numerical results presented in the following section.

However, in the three experimental results presented, the shape of the specimens considered is not prismatic. Therefore, the difference in shape could explain that, in the described conditions, the transition to the brittle behavior seems to be defined by $s \leq 1$ instead of $s \leq 0.7$. The extension of the present study with the aim of verifying the influence of the slenderness, other geometric characteristics as well as other boundary conditions will be the focus of future works.

1 **4 LDEM simulations: rock specimens with different sizes subjected to uniaxial**

2 **tensile stress**

3 **4.1 Model description**

4   A specimen group of heterogeneous material was simulated being fixed at their

5 lower face and subjected to monotonically increasing displacements at the nodes on their

6 upper faces. In all cases, nodal displacements in the normal direction to the middle surface

7 were restrained in order to simulate plane strain conditions. The specimens were analyzed

8 up to the complete failure. The specimen side b ranges between an interval of 0.05 and

9 3.50m. The smallest LDEM array that leads to satisfactory results consists of 10×10×1

10 cubic modules with 1026 DOF which were used for the smallest (0.05m) model. Whereas

11 the 3.50m model consists of 700×700×1 cubic modules with 1472802 DOF, thus,

12 constituting the largest specimen used in this study. Table 5 shows the basic dimensions

13 of the samples, while Table 6 indicates the relevant material properties.

14

15   Table 5: The dimensions of the LDEM models studied.

Specimen	1	2	3	4	5	6	7	8	9	10	11	12	13
b (m)	0.05	0.075	0.10	0.15	0.20	0.25	0.30	0.40	0.50	0.75	1.00	1.50	3.50
Cells	10	15	20	30	40	50	60	80	100	150	200	300	700

16

17   Table 6: Relevant rock (granite) material properties and LDEM parameters.

Material Properties	Value
E (Young's modulus)	75 GPa
ρ (specific mass)	2700 kg/m^3
ν (Poisson coefficient)	0.25
LDEM Properties	**Value**
L (basic modulus length)	0.005 m
d_{eq}	1.465 m
$\mu(G_f)$ (Expected value of fracture energy)	1300 N/m
$CV(G_f)$ (coefficient of variation of G_f)	40%

$\varepsilon p = 1.0878 \times 10^{-4}$

$\varepsilon r = 2.207 \times 10^{-2}$

It is important to note that in the simulations, the expected value of the fracture energy, $\mu(G_f)$, was considered as a mean value for all the sizes being simulated, instead of considering it as a variable with the size scale.

The layout of the specimens showing their relative size and boundary conditions is shown in Figure 4. It should be noticed that the fracture energy G_f is modelled as a random field using the properties indicated in Table 6. The probability distribution of G_f was considered as a Weibull function with a correlation length equal to $L_{corr} = 0.3L$, which is related to the material microstructure. As the material properties are associated with a statistical distribution, each simulation leads to a different strength and a different stress-strain curve. For this reason, four simulations were carried out for each size specimen in order to obtain representative results for each size specimen. As explained before, the correlation length used in this work is small, then the random values of G_f assigned to every bar are statistically independent, that is, the properties of one bar do not depend on the properties of the neighbor ones.

Figure 4. Relative size of the specimens and boundary conditions considered.

4.2 Results

One representative sample of the final simulated configuration for each size considered in the study is shown in Figure 5, in which the colors cyan, orange, and red represent undamaged, damaged, and totally broken (failed) elements, respectively. The sizes of the specimens are indicated in Figure 4.

The influence of the mesh discretization is studied in Refs. [46, 60], moreover, in the simulations presented here, the discretization level is similar. In addition, in Ref. [67]
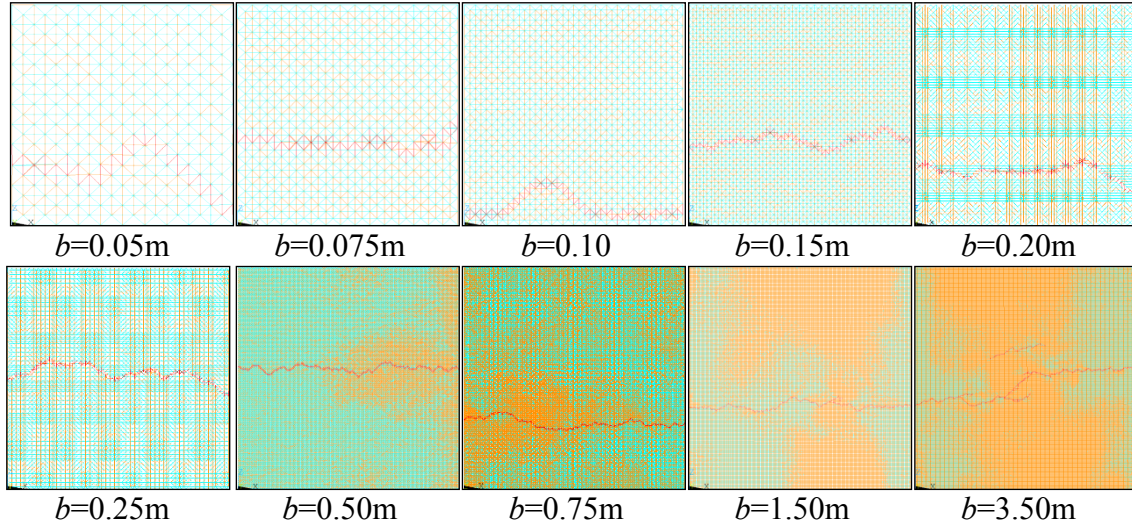
Figure 5. Damage distribution and rupture configuration of specimens of various sizes subjected to applied displacements inducing uniaxial tension. The characteristic specimen size b varies between 0.05 m and 3.5 m. The broken bars are indicated in red, the damaged bars in orange and the undamaged bars in cyan.

The resulting stress displacement curves for all simulations of the b=0.20m specimens, as well as the average curve, are shown in Figure 6. In this figure, the main parameters that characterize the stress displacement curves are represented, in which σ_p denotes the ultimate or maximum global stress, δ_c represents the critical displacement, or displacement related to ultimate stress, and δ_u represents the ultimate displacement or the displacement at the point where the strength is totally exhausted which has been defined for practical purposes as the displacement when the stress decreases below 2% of the maximum stress, σ_p. This notation is applicable without any restriction to specimens with sides smaller than 0.4m. For specimens with b equal to 0.4m or larger, failure occurs in a brittle manner and the ultimate displacement δ_u cannot be distinguished from the critical displacement δ_c. Figure 6 also shows the displacement defined as δ_{50}, that is, the displacement related to 50% of the rupture stress.
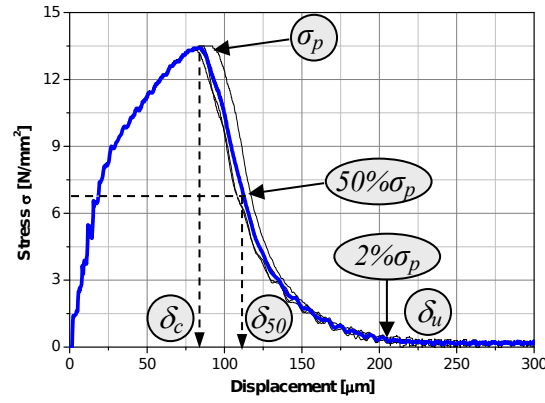
Figure 6. Curves for the mean vertical stress at lower support versus mean displacement for the b=0.20m rock specimen obtained from four simulations (black) and the average curve ones (blue).

In Figure 7(a) the global displacement versus mean stress curve for all the sizes simulated with LDEM are shown. In Fig. 7(b) the same results are presented considering the global displacement in a Log scale. In these figures, it is possible to see how the curves trend changes: specimens smaller than 0.25 m show a ductile behavior (black lines), specimens larger than 0.75 m present a brittle behavior (gray lines), whereas specimen sizes between 0.25 and 0.75 m show a transition between ductile and brittle behavior (red lines).

Figure 7. a) Displacement versus stress and b) log displacement versus stress curves for different size specimens. Ductile behavior when b<0.25 (black curves), brittle behavior when b>0.75m (gray curves), transition ductile-to- brittle behavior when b belongs to the interval [0.25, 0.75] (red curves).

1   The simulations resulted in different fracture patterns that in some cases produced

2   one, two or more cracks. It is worth noticing that the auto-similar configuration was used

3   throughout this work. For this reason, simulations, in which only one macro-crack

4   propagate, were considered. As it can be seen in Figure 5, b = 3.5m, there is more than

5   one crack in the final configuration, but the other cracks or its bifurcation become stable

6   and do not propagate to broke the specimen. When more than one crack propagates, the

7   stress-strain curves present a different morphology.

8   As shown in Figure 6, it is possible to specify the stress - displacement curves

9   through characteristic values without losing essential information. Table 7 lists the

10   correspondent characteristic mean values of the stress-displacement curves by increasing

11   the specimens' size.

12   Table 7 also presents the Carpinteri's brittleness number s obtained by Eq. (1),

13   assuming that $R = b$ the size of the specimen, and E and G_f the simulations parameters

14   presented in Table 6.

15

16   Table 7 – Mean values of peak stress, critical and rupture displacement of different
17   simulated specimen size.

b [mm]	σ_p [MPa]	CV [%]	δ_c [μm]	CV [%]	δ_u [μm]	CV [%]	δ_{50} [μm]	s Eq. (1)	s_{LDEM} Eq. (14)
50	13.461	1.10	26	7.42	225	4.53	93	3.26	5.41
75	13.518	0.85	34	7.30	211	5.01	89	2.67	4.42
100	13.415	0.98	43	5.63	207	4.08	94	2.33	3.83
150	13.508	0.63	64	0.04	213	0.14	103	1.90	3.12
200	13.473	0.39	85	3.13	213	2.44	110	1.64	2.71
250	13.429	0.68	105	1.31	203	1.76	126	1.46	2.42
300	13.393	0.16	124	0.15	185	4.77	132	1.35	2.21
400	13.488	0.31	166	1.29	184	3.33	176	1.16	1.91
500	13.471	0.30	205	1.36	228	2.41	216	1.04	1.71
750	13.455	0.39	301	1.92	322	1.72	301	0.85	1.40
1000	13.420	0.20	397	1.24	420	1.20	397	0.74	1.21
1500	13.437	0.20	605	0.76	646	0.76	605	0.60	0.99
3500	13.347	0.21	1325	1.87	1444	0.60	1325	0.39	0.65

18

19   By comparing the stress-displacement curves presented in Figure 7, it is possible to

20   identify two limits, i.e., brittleness numbers that define changes in the specimen behavior:

21   $s_{ub} \cong 1.5$ (upper bound), and $s_{lb} \cong 0.7$ (lower bound). Ductile behavior is expected for

22   $s > s_{ub}$, brittle behavior for $s_{lb} < 0.7$, and transitional behavior when $s_{lb} < s < s_{ub}$.

23   The experimental and numerical results in terms of the brittleness number s, and

24   global behavior (brittle-ductile transition), are shown in Figure 8. A global brittle

25   behavior is considered if s is smaller than 0.7, a ductile one if s is higher than 1.5. A

transition can be considered if *s* is comprised in the interval [0.7, 1.5]. It should be noted that *s* < 0.7 is a lower bound, but tests with brittle global behavior can occur with values above this limit. Furthermore, the ductile transition limit *s* > 1.5 shows a certain level of dispersion. The specimen shape and the influence of boundary conditions could be responsible for this dispersion. But despite this behavior, the limits *s*<0.7 and *s*>1.5 identify that the typical brittle-ductile transition take place in the specimens.

Figure 8: Representation of the *s* values in experimental and numerical results.

In Figure 9(a), the size effect in the mean ultimate stress is presented, and in Figure 9(b) the mean critical and ultimate displacement is also plotted. In both cases, the log scales are used to facilitate the result interpretation. A bar with +/- 2 standard deviation is included in the plots and between this bar 95% of the values obtained in the simulation are contained.

In Fig. 9(a), it is clear that the size effect in the global ultimate stress is practically null. This effect could be seen in the values presented in Table 7. The difference between the maximum and minimum values of mean global stress is 1.23% and the variation coefficients do not exceed 1.64%. The sensitivity of the global parameters with the size effect depends on several factors, such as the boundary conditions, and the random nature of the material input data. In Rios and Riera [36] experimental tests with different geometries and boundary conditions were simulated with LDEM, and the values of strength and its variability are reached with success.
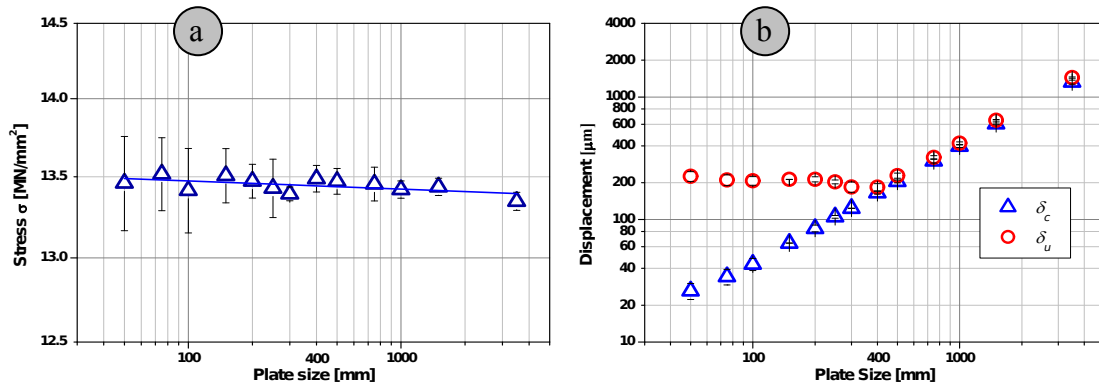
Figure 9. (a) Ultimate global stress. (b) Ultimate and characteristic global displacement versus the specimen dimension. The mean values and bar with +/- 2 standard deviation are indicated in the figure.

On the other hand, in Fig. 9(b) the specimen behavior changes in shape clearly for b =0.4 m; this result is compatible with the limits indicated in Fig. 7 and in Table 7.

A new parameter was defined to take into account the shape of the global stress versus displacement curve, or force versus displacement. The parameter proposed was the ratio δ_{50}/δ_c, between the displacement δ_{50}, when 50% of the rupture stress was reached, over the displacement δ_c, when the ultimate stress occurred. Thus, when a value of δ_{50}/δ_c is close to 1.0, a brittle behavior with unstable propagation is expected. $\delta_{50}/\delta_c>$ 1 means that the specimen will present a ductile behavior and a stable rupture is foreseen.

In Figure 10, the relation between the ratio δ_{50}/δ_c and the brittleness number s is shown for the experimental and numerical results presented in this work. In this plot, it clearly appears that for values of s higher than 1.5, ratios of δ_{50}/δ_c higher than 1.4 are obtained, therefore, indicating an evident ductile behavior for the specimen.

When s presents values between 0.7 and 1.5, the ratio δ_{50}/δ_c varies between 1.4 and 1; in these cases the specimens present a transitional ductile-to- brittle behavior.

Finally, when s is lower than 0.7, the ratio δ_{50}/δ_c will present values lower than 1.0, thus, characterizing a clear brittle behavior. It was noticed that, in this region, for several cases, the ratio δ_{50}/δ_c appears to be equal to 1.0. This is the typical value when the simulation is performed in a controlled displacement, when the specimen breaks in an unstable way and the snap-back branch of the curve is not captured. It is evident in the results of the Felser sandstone sets that, for specimens with s <1.0, a special displacement control allows to capture the snap-back branch during the softening.
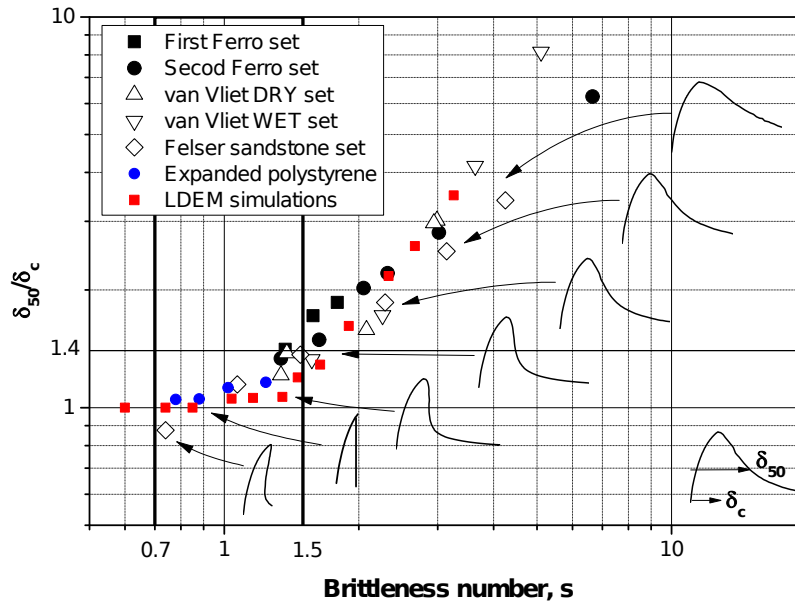
23

1

2
3 Figure 10: Relation between the Carpinteri brittleness number, *s*, and the shape of the
4 global stress - displacement curve.

5

6   Finally, the ratio between the Carpinteri's number s computed for the specimen
7 and the s_{LDEM} parameter computed in the context of the method is presented hereafter. In
8 Figure 10, the ratio s/s_{LDEM} was plotted against the ratio d_{eq}/L, the latter measuring the
9 relationship between the material length d_{eq}, that is a characteristic length of the material,
10 as defined in section 2, and the size of the element that define the level of discretization
11 used in the model.

12   In Figure 11, it is possible to verify in which way the variability of the fracture
13 energy CV (G_f) influences the brittleness number s computed using the LDEM
14 formulation. The simulations presented in section 4.1 were carried out using CV
15 (G_f)=40%, this value is usually employed to simulate quasi-brittle materials such as
16 concrete and rocks (see e.g. [36], [38]). Moreover, a particular study about the influence
17 of the variability CV (G_f) was conducted in [30].

18   The white circle in Figure 11, illustrates the LDEM simulations presented in the
19 present paper. A set of simulations presented in Ref. [50] were also added in red, together
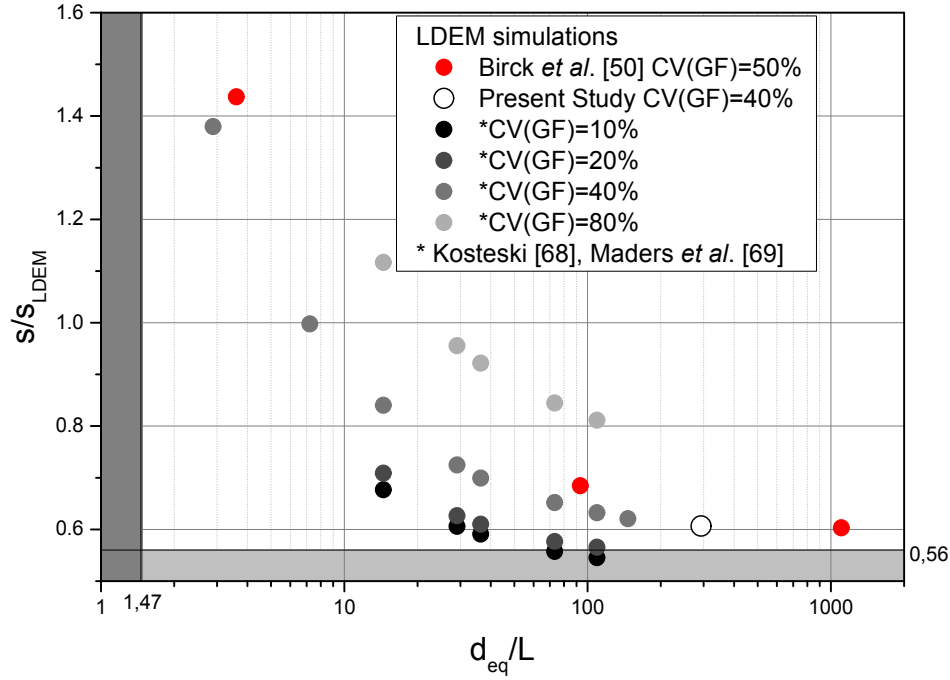20 with other results presented in Refs. [68, 69] represented by gray circles.

21

Figure 11: Relation established between the global brittleness number and the brittleness number computed in the context of LDEM versus the ratio between the equivalent d value over the element size used in the discretization.

In Figure 11, it can be noticed that an approximate relationship between s/s_{LDEM} could be considered independent of d_{eq}/L, if $d_{eq}/L > 100$ ($\varepsilon_r/\varepsilon_p \approx 60$). For lower values of this ratio, the level of the discretization influences the s/s_{LDEM} result, finding responses in the interval [0.6, 1.5]. It is also important to notice that the influence of the fracture energy variation coefficient is significant.

When an element breaks, it generates a crack with a size related to its length, L. If this crack is smaller than the material equivalent length d_{eq}, it will not propagate until it reaches this critical dimension (after nucleation). If this crack size is closed to the material equivalent length d_{eq}, then it will propagate.

A s/s_{LDEM} greater than 1 indicates that the mean axial stress of all the LDEM elements (σ_p^*) is greater than the simulation maximum global stress (σ_p). This can be found with a more "brittle" constitutive model (ε_r close to ε_p or d_{eq} close to L) and/or large dispersions in a random field. With a large dispersion, it is easier to find a less resistant element than the mean element resistance. When the element breaks, if the generated crack is of the size of d_{eq}, a brittle fracture occurs. In this case, the simulation's

25

global response is close to the resistance of this first broken element, but much smaller than the mean resistance of all the other elements together.

Conversely, a s/s_{LDEM} smaller than 1 indicates that the mean axial stress of all the LDEM elements (σ_p^*) is less than the simulation maximum global stress (σ_p). This occur when we have little dispersion of the random field (low CV) and/or a "ductile" constitutive model (ε_r much larger than ε_p or d_{eq} bigger than L).

A practical application of the graphs presented in Fig 10 to calibrate the LDEM model could be proposed:

1- If experimental data about the material are available, together with the specimen size characterized by its R, the material properties G_f, E and the stress versus displacement global curve, then the value of s can be computed using the Eq. (1).

2- Assuming that $s_{LDEM} = s$ using the Eq. (14), it is possible to obtain the material parameter d_{eq}.

3- Adopting a level of discretization and the CV(G_f) to be used in the simulation, it is possible to compute d_{eq}/L and to obtain the ratio s/s_{LDEM} using the plot presented in Fig.11.

4- With the corrected value of s_{LDEM} and using Eq. (14), a better approximation of d_{eq} could be computed.

Notice that d_{eq} is a material parameter, and for this reason, if the model calibration is performed for one specimen, this value will not vary if the geometry and boundary conditions change.

In the present paper, a comparison between the global specimen behavior during damage process and the brittleness number is established. In [42, 50, 70] the link of the brittleness number with the dissipated energy and the final configurations obtained with LDEM simulations was also studied.

5. Conclusions

In the present work, several sets of experimental and numerical results are reviewed with the aim to correlate the Carpinteri's brittleness number obtained to predict the global behavior (ductile, brittle, or ductile-to-brittle transitional behavior).

In all cases, the specimens were subjected to pure tensile stress and heterogeneous materials were also analyzed. Experimental results produced by other researchers or by the authors themselves are presented. No pre-cracked specimens were considered, that is,

the spontaneous localization of the main crack was expected. The numerical approach used was a version of the Lattice Discrete Element Method that accounts for the random nature of the material employed. With this research work, it is possible to conclude that:

- A correlation between the s number and the aspect of the global force/stress versus displacement/strain curve is evident in all the evaluated cases. For this reason, the computation of s allows to predict what kind of behavior is to be expected for each specimen.

- The values computed using experimental and numerical results allow to perceive that for the boundary conditions used, when s <0.7 is used as a lower bound, a global brittle behavior is expected. On the other hand, if s >1.5, a ductile behavior is expected, moreover, in the interval of s [0.7, 1.5], a ductile-to-brittle transitional behavior occurs. The extension of the present study to verify the influence of the boundary condition and the specimen geometry will be the focus of future works.

- The relationship between the traditional definition of s and the definition of the brittleness number computed in the context of the numerical method used, s_{LDEM}, was presented. This relationship can be used to calibrate, in a consistent way, the LDEM method employed. It is possible to extend this methodology of calibration to other versions of the discrete element method (for example in Perydinamics), where spontaneous fracture can be also simulated.

- The satisfactory correlation between experimental and LDEM results confirms the robustness of this method as a numerical tool to model fracture processes in quasi-brittle materials.

REFERENCES

[1] Dugdale DS. Yielding of steel sheets containing slits. J Mech Phys Solids. 1960, 8:2, 100-104. https://doi.org/10.1016/0022-5096(60)90013-2.

[2] Boyle RW, Sullivan AM, Krafft JM. Determination of plane strain fracture toughness with sharply notched sheets. Welding J Res Suppl. 1962, 41, 428-432.

[3] Brown Jr WF, Srawley JE. Plane strain crack toughness testing of high strength metallic materials. ASTM Special Technical publication, No. 410, ASTM, Philadelphia, Pa. 1966.

[4] Mpalaskas AC, Matikas TE, Van Hemelrijck D, Papakitsos GS, Aggelis DG. Acoustic emission monitoring of granite under bending and shear loading. Archives of Civil and Mechanical Engineering. 2016, 16: 3, 313-324. https://doi.org/10.1016/j.acme.2016.01.006

[5] Mpalaskas AC, Thanasia OV, Matikas TE, Aggelis DG. Mechanical and fracture behavior of cement-based materials characterized by combined elastic wave approaches. Construction and Building Materials. 2014, 50, 649-656. https://doi.org/10.1016/j.conbuildmat.2013.10.022

[6] Carpinteri A. Static and energetic fracture parameters for rocks and concretes. Mat Constr. 1981, 14:81, 151-162. https://doi.org/10.1007/BF02473919.

[7] Carpinteri A. Application of fracture mechanics to concrete structures. Journal of the Structural Division (ASCE). 1982, 108: 4, 833-848.

[8] Carpinteri A. Post-peak and post-bifurcation analysis of cohesive crack propagation. Eng Fract Mech. 1989, 32: 2, 265-278. https://doi.org/10.1016/0013-7944(89)90299-3

[9] Carpinteri A. Cusp catastrophe interpretation of fracture instability. Journal of the Mechanics and Physics of Solids. 1989, 37: 5, 567-582. https://doi.org/10.1016/0022-5096(89)90029-X.

[10] Carpinteri A, Marenga C, Savadori A. Ductile-brittle transition by varying structural size. Eng Fract Mech. 1985, 21, 263-271. https://doi.org/10.1016/0013-7944(85)90015-3

[11] Carpinteri A. Scaling laws and renormalization groups for strength and toughness of disordered materials. Int J Solids Struct, 1994, 31(3), 291-302. https://doi:10.1016/0020-7683(94)90107-4

[12] Carpinteri A, Marega C, Savadori A. Size effects and ductile-brittle transition of polypropylene. J Mater Sci. 1986, 21: 4173-4178. https://doi.org/10.1007/BF01106526.

[13] Carpinteri A, Cornetti P, Barpi F, Valente S. Cohesive crack model description of ductile to brittle size-scale transition: dimensional analysis vs. renormalization group theory. Eng Fract Mech, 2003, 70, 1809-1839. https://doi.org/10.1016/S0013-7944(03)00126-7

[14] Brincker R, Henriksen MS, Christensen FA, Heshe G. Size Effects on the Bending Behaviour of Reinforced Concrete Beams. European Structural Integrity Society. 1999, 24, 127-137. https://doi.org/10.1016/S1566-1369(99)80064-8

[15] Gao H. Application of fracture mechanics concepts to hierarchical biomechanics of bone and bone-like materials. Int J Fract. 2006, 138, 101-137. https://doi.org/10.1007/s10704-006-7156-4.

[16] Corrado M, Cadamuro E, Carpinteri A. Dimensional analysis approach to study snap back-to-softening-to-ductile transitions in lightly reinforced quasi-brittle materials. A. Int J Fract. 2011, 172:1, 53-63. https://doi.org/10.1007/s10704-011-9646-2.

[17] Krajcinovic D. Damage Mechanics. Elsevier, Amsterdam, 1986.

[18] Seleson P, Beneddine S, Prudhomme S. A force-based coupling scheme for peridynamics and classical elasticity. Comp Mat Sci. 2013, 66, 34-49. https://doi.org/10.1016/j.commatsci.2012.05.016.

[19] Silling SA. Reformulation of elasticity theory for discontinuities and long-range forces. J Mech Phys Solids. 2000, 48, 175-209. https://doi.org/10.1016/S0022-5096(99)00029-0.

[20] Schlangen E, van Mier JGM. Crack propagation in sandstone: Combined experimental and numerical approach. Rock Mech Rock Engng. 1995, 28, 93-110. https://doi.org/10.1007/BF01020063.

[2] Krajcinovic D, Vujosevic M. Strain localization-short to long correlation length transition. Int J Solids Struct. 1998, 35, 31-32. https://doi.org/10.1016/S0020-9683(97)00307-7

[22] Sagar RV, Raghu Prasad BK. Modeling heterogeneity of concrete using 2D lattice network for concrete fracture and comparison with AE study. Sadhana. 2009, 34, 865-886. https://doi.org/10.1007/s12046-009-0052-7.

[23] Nagy E, Landis EN, Davids WG. Acoustic emission measurements and lattice simulations of microfracture events in spruce. Holzforschung, 2010, 64, 455-461. https://doi.org/10.1515/hf.2010.088.

[24] Rinaldi A. Advances in Statistical Damage Mechanics (SDM): New Modeling Strategies. In: Damage Mechanics and Micromechanics of Localized Fracture Phenomena in Inelastic Solids. CISM Courses and Lectures, vol 525. Springer, Vienna, 2011.

[25] Mastilovic S, Rinaldi A. Two-Dimensional Discrete Damage Models: Discrete Element Methods, Particle Models, and Fractal Theories. In: Voyiadjis G. (eds) Handbook of Damage Mechanics. Springer, New York, NY, 2015, 273-303.

[26] Riera JD. Local effects in impact problems on concrete structures. Proceedings of the Conference on Structural Analysis and Design of Nuclear Power Plants vol 3, Porto Alegre, October 3-5, 1984.

[27] Riera JD, Iturrioz I. Discrete element dynamic response of elastoplastic shells subjected to impulsive loading. Commun Numer Meth En. 1995, 11, 417-426. https://doi.org/10.1002/cnm.1640110506.

[28] Riera JD, Iturrioz I. Discrete element model for evaluating impact and impulsive response of reinforced concrete plates and shells subjected to impulsive loading. Nucl Eng Des. 1998, 179, 135-144. https://doi.org/10.1016/S0029-5493(97)00270-7.

[29] Kosteski LE, Riera JD, Iturrioz I, Singh RK, Kant T. Analysis of reinforced concrete plates subjected to impact employing the truss-like discrete element method. Fatigue Fract Eng M. 2015, 38, 276-289. https://doi.org/10.1111/ffe.12227.

[30] Kosteski LE, Iturrioz I, Cisilino AP, Barrios D'ambra R, Pettarin V, Fasce L, Frontini P. A lattice discrete element method to model the falling-weight impact test of PMMA specimens. Int J Impact Eng. 2016, 87, 120-131. https://doi.org/10.1016/j.ijimpeng.2015.06.011

[31] Schnaid F, Spinelli L, Iturrioz I, Rocha M. Fracture mechanics in ground improvement design. Ground Improvement. 2004, 8, 7-15. https://doi.org/10.1680/grim.2004.8.1.7

[32] Dalguer LA, Irikura K, Riera JD, Chiu HC. The importance of the dynamic source effects on strong ground motion during the 1999 Chi-Chi, Taiwan, Earthquake: Brief Interpretation of the Damage Distribution on Buildings. Bull Seismol Soc Am. 2001, 91: 5, 1112-1127. https://doi.org/10.1785/0120000705

[33] Dalguer LA, Irikura K, Riera JD. Simulation of tensile crack generation by three-dimensional dynamic shear rupture propagation during an earthquake. J Geophys Res. 2003, 108, No. B3, 2144. https://doi.org/10.1029/2001JB001738

[34] Iturrioz I, Birck G, Riera JD. Numerical DEM simulation of the evolution of damage and AE preceding failure of structural components. Eng Fract Mech. 2019, 210, 247-256 doi.org/10.1016/j.engfracmech.2018.02.023.

[35] Birck G, Riera JD, Iturrioz I. Numerical DEM simulation of AE in plate fracture and analogy with the frequency of seismic events in SCRs. Eng Fail Anal. 2018, 93, 214-223. https://doi.org/10.1016/j.engfailanal.2018.06.024

[36] Rios RD, Riera JD. Size effects in the analysis of reinforced concrete structures. Eng Struc. 2004, 26, 1115-1125. https://doi.org/10.1016/j.engstruct.2004.03.012

[37] Iturrioz I, Morquio A, Bittencourt E, Rosito d´Avila V. Performance of the Discrete Element Method to represent the scale effect. Published in Mechanics of Solids in Brazil 2007, Brazilian Society of Mechanical Sciences and Engineering. ISBN 978-85-85769-30-7, 2007, 247- 263.

[38] Iturrioz I, Miguel LFF, Riera JD. Dynamic fracture analysis of concrete or rock plates by means of the Discrete Element Method. Lat Am J Solids Stru. 2009, 6, 229-245.

[39] Iturrioz I, Riera JD, Miguel LFF, Kosteski LE. Scale Effects in Quasi-Fragile Materials Subjected to Compress. IASMiRT, SMiRT 21 - New Delhi, India. November 6-11, 2011

[40] Miguel LFF, Riera JD, Iturrioz I. Influence of size on the constitutive equations of concrete or rock dowels. Int J Numer Anal Meth Geomech. 2008, 32, 1857-1881. https://doi.org/10.1002/nag.699.

[41] Miguel LFF, Iturrioz I, Riera JD. Size effects and mesh independence in dynamic fracture analysis of brittle materials. CMES, 2010, 56, 1-16. 10.3970/cmes.2010.056.001

[42] Colpo AB, Kosteski LE, Iturrioz I. The size effect in quasi-brittle materials: Experimental and numerical analysis. Int J Dam Mech. 2017, 26, 395-416. https://doi.org/10.1177/1056789516671776.

[43] Kosteski LE, Barrios D'Ambra R, Iturrioz I. Determinación de parámetros fractomecánicos estáticos y dinámicos utilizando el método de los elementos discretos compuestos por barras. Rev int métodos numér cálc diseño ing. 2008, 24: 4, 323-343. URL https://www.scipedia.com/public/Kosteski_et_al__2008a.

[44] Kosteski LE, Barrios D'Ambra R, Iturrioz I. Fractomechanics parameter calculus using the Discrete Element Method. Lat Am J Solids Stru. 2010, 6, 301-321.

[45] Kosteski LE, Iturrioz I, Batista RG, Cisilino AP. The truss-like discrete element method in fracture and damage mechanics. Eng Computations. 2011, 28, 765-787. https://doi.org/10.1108/02644401111154664.

[46] Kosteski LE, Barrios D'Ambra R, Iturrioz I. Crack propagation in elastic solids using the truss-like discrete element method. I Int J Fract. 2012, 174, 139-161. https://doi.org/10.1007/s10704-012-9684-4.

[47] Riera JD, Miguel LFF, Iturrioz I. Strength of Brittle Materials under high strain rates in DEM simulations. CMES, 2011, 82, 113-136. 10.3970/cmes.2011.082.113

[48] Iturrioz I, Lacidogna G, Carpinteri A. Experimental analysis and truss-like discrete element model simulation of concrete specimens under uniaxial compression. Eng Fract Mech. 2013, 110, 81-98. https://doi.org/10.1016/j.engfracmech.2013.07.011

[49] Iturrioz I, Lacidogna G, Carpinteri A. Acoustic emission detection in concrete specimens: Experimental analysis and lattice model simulations. Int J Dam Mech. 2014, 23, 327-358. https://doi.org/10.1177/1056789513494232

[50] Birck G, Iturrioz I, Lacidogna G, Carpinteri A. Damage process in heterogeneous materials analyzed by a lattice model simulation. Eng Fail Anal. 2016, 70, 157-176. https://doi.org/10.1016/j.engfailanal.2016.08.004

[51] Da Silva GS, Kosteski LE, Iturrioz I. Analysis of the failure process by using the Lattice Discrete Element Method in the Abaqus environment. Theoretical and Applied Fracture Mechanics. 2020, 107, 102563. https://doi.org/10.1016/j.tafmec.2020.102563

[52] Nayfeh AH, Hefzy MS. Continuum modeling of three-dimensional truss-like space structures. AIAA Journal. 1978, 16, 779-787. https://doi.org/10.2514/3.7581

[53] Rinaldi A, Krajcinovic D, Peralta P, Lai YC. Lattice models of polycrystalline microstructures: a quantitative approach. Mech Mater. 2008, 40, 17-36. https://doi.org/10.1016/j.mechmat.2007.02.005.

[54] Rocha MM, Riera JD, Krutzik NJ. Extension of a model that aptly describes fracture of plain concrete to the impact analysis of reinforced concrete. Int. Conf. and Structural Mechanics in Reactor Technology, SMiRT 11, Trans. Vol. J., Tokyo, Japan. 1991.

[55] Hillerborg A. A model for fracture analysis. Cod LUTVDG/TV BM-3005, 1-8. 1978.

[56] Kupfer HB, Gerstle KH. Behavior of concrete under biaxial stresses. J Eng Mech Div. 1973, 99: 4, 853-866.

[57] Kanninen MF, Popelar CH. Advanced Fracture Mechanics. Oxford University Press. 1985. ISBN 0-19-503532-1.

[58] Silling SA, Epton M, Weckner O, Xu J, Askari E. Peridynamic States and Constitutive Modeling. J Elasticity, 2007, 88, 151-184. https://doi.org/10.1007/s10659-007-9125-1

[59] Taylor D. The Theory of Critical Distances: A New Perspective in Fracture Mechanics, Elsevier. 2007.

[60] Puglia VB, Kosteski LE, Riera JD, Iturrioz I. Random field generation of the material properties in the lattice discrete element method. J Strain Anal Eng, 2019, 54: 4, 236-246 https://doi.org/10.1177/0309324719858849

[61] Iturrioz I, Riera JD, Miguel LFF. Introduction of imperfections in the cubic mesh of the truss-like discrete element method. Fatigue Fract Eng M. 2014, 37: 5, 539-552. https://doi.org/10.1111/ffe.12135

[62] Carpinteri A, Ferro G. Size effects on tensile fracture properties: A unified explanation based on disorder and fractality of concrete microstructure. Mater Struct. 1994, 27, 563-571. https://doi.org/10.1007/BF02473124

[63] Carpinteri A, Ferro G. Scaling behaviour and dual renormalization of experimental tensile softening responses, Mat. Struct. 1998, 31, 303-309. https://doi.org/10.1007/BF02480671

[64] van Vliet MRA. Size effect in tensile fracture of concrete and rock. Ph.D. Thesis, Delft University of Technology, Delft, The Netherlands. 2000.

[65] van Vliet MRA, van Mier JGM. Size effects of concrete and sandstone. Heron, 2000, 45, 91-108. http://resolver.tudelft.nl/uuid:f2beb295-f41d-4db1-b126-8be73c23317b

[66] Carpinteri A, Maradei F. Three-jack solution to obtain a truly stable and symmetric tensile concrete test. Experimental Mechanics. 1995, 35, 19-23. https://doi.org/10.1007/BF02325829

[67] Birck G, Iturrioz I, Riera JD, Miguel LFF. Influence of mesh orientation in discrete element method simulations of fracture processes. J Strain Anal Eng Des. 2018, 53: 6, 400-407. https://doi.org/10.1177/0309324718775284

[68] Kosteski LE. Aplicação do Método dos Elementos Discretos formado por barras no estudo do colapso de estruturas. Doctoral Thesis, Universidade Federal de Rio Grande do Sul, Porto Alegre, 2012 (in Portuguese). http://hdl.handle.net/10183/56589

[69] Maders L, Kosteski LE, Iturrioz I. Estudo do efeito de escala no método dos elementos discretos formado por barras. In: Mecom 2012, Salta, Argentina. Mecánica Computacional v. XXXI, 1857-1876.

[70] Birck G, Rinaldi A, Iturrioz I. The fracture process in quasi-brittle materials simulated using a lattice dynamical model. Fatigue Fract Eng Mater Struct. 2019, 42: 12, 2709-2724. https://doi.org/10.1111/ffe.13094